On the ability of RegCM4 regional climate model to simulate surface solar radiation patterns over Europe: An assessment using satellite-based observations

G. Alexandri[1,2*], A. K. Georgoulias[3,4,5], P. Zanis[3], E. Katragkou[3], A. Tsikerdekis[3], K. A. Kourtidis[2], C. Meleti[1]

[1] Laboratory of Atmospheric Physics, Physics Department, Aristotle University of Thessaloniki, 54124, Thessaloniki, Greece

[2] Laboratory of Atmospheric Pollution and Pollution Control Engineering of Atmospheric Pollutants, Department of Environmental Engineering, Democritus University of Thrace, 67100, Xanthi, Greece

[3] Department of Meteorology and Climatology, School of Geology, Aristotle University of Thessaloniki, 54124, Thessaloniki, Greece

[4] Multiphase Chemistry Department, Max Planck Institute for Chemistry, D-55128, Mainz, Germany

[5] Energy, Environment and Water Research Center, The Cyprus Institute, Nicosia Cyprus

Correspondence to: G. Alexandri (alexang@auth.gr)

Abstract

In this work, we assess the ability of RegCM4 regional climate model to simulate surface solar radiation (SSR) patterns over Europe. A decadal RegCM4 run was implemented and evaluated against satellite-based observations from the Satellite Application Facility on Climate Monitoring (CM SAF) showing that the model simulates adequately the SSR patterns over the region. The SSR bias between RegCM4 and CM SAF is +1.5% for MFG (Meteosat First Generation) and +3.3% for MSG (Meteosat Second Generation) observations. The relative contribution of parameters that determine the transmission of solar radiation within

the atmosphere to the deviation appearing between RegCM4 and CM SAF SSR is also examined. Cloud macrophysical and microphysical properties such as cloud fractional cover (CFC), cloud optical thickness (COT) and cloud effective radius (Re) from RegCM4 are evaluated against data from CM SAF. Generally, RegCM4 underestimates CFC by 24.3% and Re for liquid/ice clouds by 36.1%/28.3% and overestimates COT by 4.3%. The same procedure is repeated for aerosol optical properties such as aerosol optical depth (AOD) asymmetry factor (ASY) and single scattering albedo (SSA), as well as other parameters including surface broadband albedo (ALB) and water vapor amount (WV) using data from MACv1 aerosol climatology, from CERES satellite sensors and from ERA-Interim reanalysis. It is shown here that the good agreement between RegCM4 and satellite-based SSR observations can be partially attributed to counteracting effects among the above mentioned parameters. The potential contribution of each parameter to the RegCM4-CM SAF SSR deviations is estimated with the combined use of the aforementioned data and a radiative transfer model (SBDART). CFC, COT and AOD are the major determinants of these deviations on a monthly basis; however, the other parameters also play an important role for specific regions and seasons. Overall, for the European domain, CFC, COT and AOD are the most important factors, since their underestimations and overestimations by RegCM4 cause an annual RegCM4-CM SAF SSR absolute deviation of 8.4%, 3.8% and 4.5%, respectively.

1   Introduction

Modeling climate on a regional scale is essential for assessing the impact of climate change on society, economy and natural resources. Regional climate models are limited-area models that simulate climate processes being often used to downscale dynamically global model simulations or global reanalysis data for specific regions in order to provide more detailed results (Laprise, 2008; Rummukainen, 2010). Several studies suggest that we can benefit from the use of regional climate models, especially due to the higher resolution of stationary features like topography, coastlines and from the improved representation of small-scale processes such as convective precipitation (see Flato et al., 2013 and references therein). Usually, regional climate models are evaluated and "tuned" according to their ability to simulate temperature and precipitation (e.g. Giorgi et al., 2012; Vautard et al., 2013; Kotlarski et al., 2014). However, as discussed in Katragkou et al. (2015), the role of other

1 climatological parameters should be included in the evaluation procedure of regional climate

2 models (e.g. radiative fluxes, sensible and latent heat fluxes and cloud properties).

3 The ability of regional climate models to assess surface solar radiation (SSR) patterns has not

4 received so much attention despite the fact that SSR plays a core role in various climatic

5 processes and parameters such as: 1) evapotranspiration (e.g. Teuling et al., 2009), 2)

6 hydrological cycle (e.g. Allen & Ingram, 2002; Ramanathan et al., 2001; Wang et al., 2010;

7 Wild and Liepert, 2010), 3) photosynthesis (e.g. Gu et al., 2002; Mercado et al., 2009), 4)

8 oceanic heat budget (e.g. Lewis et al., 1990; Webster et al., 1996; Bodas-Salcedo et al., 2014),

9 5) global energy balance (e.g. Kim and Ramanathan, 2008; Stephens et al., 2012; Trenberth et

10 al., 2009; Wild et al., 2013) and solar energy production (Hammer et al., 2003) and largely

11 affects temperature and precipitation. The same stands for the parameters that drive SSR

12 levels, such as cloud macrophysical and microphysical properties (cloud fractional cover

13 CFC, cloud optical thickness COT and cloud effective radius Re), aerosol optical properties

14 (aerosol optical depth AOD, asymmetry factor ASY and single scattering albedo SSA),

15 surface broadband albedo (ALB) and atmospheric water vapor amount (WV). However,

16 during the last years, there were a few regional climate model studies focusing on the SSR

17 levels or the net surface shortwave radiation, either to examine the dimming/brightening

18 effect (e.g. Zubler et al., 2011; Chiacchio et al., 2015) or to evaluate the models (e.g. Jaeger et

19 al., 2008; Markovic et al., 2008; Kothe and Ahrens, 2010; Kothe et al., 2011; 2014; Güttler et

20 al., 2014). These studies highlight the dominating effect of cloud cover and surface albedo.

21 In this work, we go a step further, proceeding to a detailed evaluation of the ability of

22 RegCM4 regional climate model to simulate SSR patterns over Europe taking into account

23 not only CFC and ALB but also COT, Re, AOD, ASY, SSA and WV. For the scopes of this

24 study, the same parameters are extracted from satellite-based observational data (CM SAF,

25 CERES), data from an aerosol climatology (MACv1) and data from the ERA-Interim

26 reanalysis (see Table 1). First a decadal simulation (2000-2009) is implemented with the

27 model and the output is evaluated against observations from the EUMETSAT geostationary

28 satellites of CM SAF. SSR data from the Meteosat First Generation (MFG) satellites (Tessier

29 et al., 1989) are available for the period 2000-2005 while data from the Meteosat Second

30 Generation (MSG) satellites (Schmetz et al., 2002) are available for the period 2006-2009.

31 These data are characterized by a high spatial (~3-5 km) and temporal resolution (15-30 min)

32 and have been validated in the past, constituting a well-established product (e.g. Sanchez-

Lorenzo et al., 2013; Posselt et al., 2014). In Sect. 2.1., the basic features of the model are described along with the simulation setup and the way various parameters are calculated by the model. In Sects. 2.2. and 2.3., a description of the satellite data from CM SAF and the other data which are used for the evaluation of RegCM4 is given, while, in Sect. 2.4., we discuss the methodology followed in this manuscript. Sect. 3.1. includes the evaluation of RegCM4 SSR against data from MFG and MSG, Sect. 3.2. and 3.3. the evaluation of CFC, COT and Re against data from MSG, Sect 3.4. the comparison of RegCM4 AOD, ASY and SSA with data from MACv1 aerosol climatology and Sect 3.5. the comparison of RegCM4 WV and ALB with data from ERA-Interim reanalysis and CERES satellite sensors, respectively. The CFC, COT, Re, AOD, ASY, SSA, ALB and WV datasets where chosen so as to be consistent with the CM SAF SSR dataset. The potential contribution of various parameters to the RegCM4-CM SAF SSR differences is estimated with the combined use of the data mentioned above and a radiative transfer model for the MSG SSR period (2006-2009). The results are presented in Sect. 3.6., while the main findings of this manuscript are summarized in Sect.4.

2   Model description, data and methods

2.1   RegCM4 description and simulation setup

In this work, a decadal (2000-2009) simulation was implemented with RegCM4.4 (hereafter denoted as RegCM4 or RegCM) for the greater European region with an horizontal resolution of 50 km. The model's domain extends from 65° W to 65° E and 15° N to 75° N including the largest part of the Sahara Desert and part of Middle East (see Fig. S1 in the Supplement of this manuscript). RegCM is a hydrostatic, sigma-p regional climate model with a dynamical core based on the hydrostatic version of NCAR-PSU's Mesoscale Model version 5 (MM5) (Grell et al., 1994). Specifically, RegCM4 is a substantially improved version of the model compared to its predecessor RegCM3 (Pal et al., 2007) by means of software code and physics (e.g. radiative transfer, planetary boundary layer, convection schemes over land and ocean, land types and surface processes, ocean-air exchanges). Details on the historical evolution of RegCM from the late 1980s until today and a full description of RegCM4's basic features are given in Giorgi et al. (2012).

1   Data from ECMWF's ERA-Interim reanalysis were used as lateral boundary conditions.

2   RegCM4 through a simplified aerosol scheme accounts for anthropogenic SO_2, sulfates,

3   organic and black carbon (Solmon et al., 2006). The emissions of these anthropogenic

4   aerosols are based on monthly, timed-dependent, historical emissions from the Coupled

5   Model Intercomparison Project Phase 5 (CMIP5) (Lamarque et al., 2010) with one year spin

6   up time (1999). This inventory is used by a number of climate models in support of the most

7   recent report of the Intergovernmental Panel on Climate Change (IPCC, 2013). The model

8   also accounts for maritime particles through a 2-bin sea salt scheme (Zakey et al., 2008) and

9   for dust through a 4-bin approach (Zakey et al., 2006). For each model layer a concentration

10 of anthropogenic SO_2, sulfates, black carbon, organic carbon, sea-salt particles and dust is

11 calculated, from which according to a look-up table with associated optical properties, the

12 model accounts for the aerosol extinction profiles (see Solmon et al., 2006; Zakey et al., 2006;

13 2008 for more details). For our simulation, the MIT-Emanuel convection scheme (Emanuel,

14 1991; Emanuel and Zivkovic-Rothman, 1999) was used. Convection is triggered when the

15 buoyancy level is higher than the cloud base level. The cloud mixing is considered to be

16 episodic and inhomogenous while the convective fluxes are based on a model of sub-cloud-

17 scale updrafts and downdrafts (see Giorgi et al., 2012). Zanis et al. (2009) reported for

18 RegCM3 that the low stratiform clouds are systematically denser and more persistent with the

19 use of the Grell (Grell, 1993) convective scheme than with the Emannuel scheme, a result

20 with major importance for the cloud- radiation feedback. The boundary layer scheme of

21 Holtslag et al. (1990) was utilized while the Subgrid Explicit Moisture Scheme (SUBEX)

22 handles large-scale cloud and precipitation computations. The ocean flux scheme was taken

23 from Zeng et al. (1998) with the Biosphere-Atmosphere Transfer Scheme (BATS) (Dickinson

24 et al., 1993) accounting for land surface processes.

25 The Community Climate Model version 3 (CCM3) (Kiehl et al., 1996) radiative package

26 handles radiative transfer within RegCM4. The CCM3 scheme employs the δ-Eddington

27 approximation following its predecessor (CCM2) (Briegleb, 1992). Especially for the

28 shortwave radiation, the radiative transfer model takes into account the effect of atmospheric

29 water vapor and greenhouse gasses, aerosol amount and optical properties (e.g. aerosol optical

30 thickness, asymmetry factor, single scattering albedo) as well as cloud macrophysical (e.g.

31 cloud fractional cover) and microphysical properties per layer (e.g. effective droplet radius,

32 liquid water path, cloud optical thickness) and land surface properties (surface albedo). The

1 radiative transfer equation is solved for 18 discrete spectral intervals from 0.2 to 5 μm for the

2 18 RegCM vertical sigma layers from 50 hPa to the surface.

3 The effect of clouds on shortwave radiation is manifested by CFC, cloud droplet size and

4 cloud water path (CWP) which is based on the prognostically calculated parameter of cloud

5 water amount (Giorgi et al., 2012). Within the model, the effective droplet radius for liquid

6 clouds (Rel) is considered constant (10 μm) over the ocean while over land it is given as a

7 function of temperature (Kiehl et al., 1998; Collins et al., 2004). On the other hand, the ice

8 particle effective radius (Rei) is given as a function of normalized pressure, starting from 10

9 μm. The equations used for the calculation of Rel and Rei are given below.

10

$$
11 \quad \mathrm{Re}\,l = \begin{cases} 5\,\mu m & T > -10^{o}C \\ 5 - 5\left(\dfrac{T+10}{20}\right)\mu m & -30^{o}C \le T \le -10^{o}C \\ \mathrm{Re}\,i & T < -30^{o}C \end{cases} \qquad (1)
$$

12

$$
13 \quad \mathrm{Re}\,i = \begin{cases} \mathrm{Re}\,i_{min} & p/p_s > p_I^{high} \\ \mathrm{Re}\,i_{min} - (\mathrm{Re}\,i_{max} - \mathrm{Re}\,i_{min})\left[\dfrac{(p/p_s) - p_I^{high}}{p_I^{high} - p_I^{low}}\right]\mu m & p/p_s \le p_I^{high} \end{cases} \qquad (2)
$$

14

15 where T is the atmospheric temperature, p is the atmospheric pressure, p_s is the surface

16 pressure, $\mathrm{Re}i_{max}$=30 μm, $\mathrm{Re}i_{min}$=10 μm, p_I^{high}=0.4 and p_I^{low}=0.0.

17 The fraction (f_{ice}) of cloud water that consists of ice particles is given as a function of T, the

18 fraction (f_{liq}) of the liquid water droplets being calculated as f_{liq}=1-f_{ice}.

19

$$
20 \quad f_{ice} = \begin{cases} 0 & T > -10^{o}C \\ -0.05(T+10) & -30^{o}C \le T \le -10^{o}C \\ 1 & T < -30^{o}C \end{cases} \qquad (3)
$$

21

6

1   Then, the radiative properties of liquid and ice clouds in the shortwave spectral region are

2   given by the following parameterizations, originally found in Slingo (1989) and revisited by

3   Briegleb et al. (1992).

4

$$COT_{ph}^{\lambda} = CWP \left[a_{ph}^{\lambda} + \frac{b_{ph}^{\lambda}}{Re_{ph}} \right] f_{ph} \tag{4}$$

$$SSA_{ph}^{\lambda} = 1 - c_{ph}^{\lambda} - d_{ph}^{\lambda} \, Re_{ph} \tag{5}$$

$$ASY_{ph}^{\lambda} = e_{ph}^{\lambda} + f_{ph}^{\lambda} \, Re_{ph} \tag{6}$$

$$\varphi_{ph}^{\lambda} = (ASY_{ph}^{\lambda})^2 \tag{7}$$

9

10   where superscript λ denotes the spectral interval and subscript ph denotes the phase

11   (liquid/ice) while φ is the phase function of clouds. It has to be highlighted here that all the

12   equations presented above are given in Kiehl et al. (1998) and Collins et al. (2004) with a

13   slightly different annotation. The coefficients a-f for liquid clouds are given in Slingo (1989),

14   while for ice clouds in Ebert and Curry (1992) for the four pseudo-spectral intervals (0.25-

15   0.69, 0.69-1.19, 1.19-2.38 and 2.38-4.00 μm) employed in the radiative scheme of RegCM.

16   Especially for COT, in this paper we calculated it for the spectral interval 0.25-0.69 μm for

17   both liquid and ice clouds so as to be comparable to the CM SAF satellite retrieved COT at

18   0.6 μm (see Sect. 2.2.). Following the approach of Cess (1985), to derive the bulk COT for the

19   whole atmospheric column, the COTs calculated for each layer are simply added. The total

20   COT for each layer is calculated by merging the COT values for liquid and ice clouds.

21   Within RegCM, CFC at each layer is calculated from relative humidity and cloud droplet

22   radius. The surface radiation flux in RegCM4 is calculated separately for the clear and cloud

23   covered part of the sky. The total CFC for each model grid-cell is an intermediate value

24   between the one calculated using the random overlap approach, which leads to a maximum

25   cloud cover, and the one found by assuming a full overlap of the clouds appearing in different

26   layers, which minimizes cloud cover. As discussed in Giorgi et al. (2012), this approach

27   allows for a more realistic representation of surface radiative fluxes.

2.2 CM SAF satellite data

To evaluate the RegCM4 SSR simulations described previously, we use high resolution satellite data from the SIS (Surface Incoming Shortwave radiation) product of CM SAF. The datasets were obtained from EUMETSAT's MFG (DOI:10.5676/EUM_SAF_CM/RAD_MVIRI/V001) and MSG (DOI:10.5676/EUM_SAF_CM/CLAS/V001) geostationary satellites. SSR data are available from 1983 to 2005 from six Meteosat First Generation satellites (Meteosat 2-7) and from 2005 onwards from Meteosat Second Generation satellites (Meteosat 8-10). These satellites fly at an altitude of ~36000 km, being located at longitudes around 0° above the equator and covering an area extending from 80° W to 80° E and from 80° S to 80° N. In the case of MFG satellites, the SSR data are retrieved from measurements with the Meteosat Visible and Infrared Instrument (MVIRI) sensor. MVIRI is a radiometer that takes measurements at 3 spectral bands (visible, water vapor, infrared) every 30 minutes. SSR is retrieved using MVIRI's broadband visible channel (0.45-1 μm) only, at a spatial resolution of ~2.5 km (at the sub-satellite point). The data are afterwards re-gridded at a 0.03^o x 0.03^o regular grid.

The MagicSol-Heliosat algorithm, used for the derivation of the SSR data analyzed in this work, has been extensively described in several papers (see Posselt et al., 2011a,b; Mueller et al., 2011; Posselt et al., 2012; Sanchez-Lorenzo et al., 2013; Posselt et al., 2014). The algorithm includes a modified version of the original Heliosat method (Beyer et al., 1996; Cano et al., 1986). Heliosat utilizes the digital counts obtained from the visible channel to calculate the so-called effective cloud albedo. The modified version incorporates the determination of the monthly maximum normalized digital count (for each MVIRI sensor) that serves as a self-calibration parameter. To derive the clear-sky background reflection, a 7-day running average of the minimum normalized digital counts is used instead of fixed monthly mean values. This method minimizes changes appearing in the radiance data recorded by different MVIRI sensors due to the transition from the one Meteosat satellite to the other, ensuring an as much as possible homogeneous dataset. Then, the clear-sky irradiances are derived using the look-up-table based clear-sky model MAGIC (Mueller et al., 2009) and finally SSR is retrieved by combining them with the effective cloud albedo.

On the other hand, MSG satellites carry the Spinning Enhanced Visible and Infrared Imager (SEVIRI), a radiometer taking measurements at 12 spectral bands (from visible to infrared) every 15 minutes with a spatial resolution of ~3 km (at the sub-satellite point). The data used

here are available at a 0.05° x 0.05° regular grid. The SEVIRI broadband high-resolution visible channel (HRV) which is very close to MVIRI's broadband visible channel cannot be used for the continuation of the SSR dataset, since, unlike MVIRI, it does not cover the full earth's disk. On the other hand, the use of one of the SEVIRI's narrow band visible channels directly in the same algorithm as MVIRI (MagicSol) is not feasible, first of all, because of the spectral differences with MVIRI's broadband visible channel, and second, because of the sensitivity of cloud albedo to spectral differences of the land surfaces below the clouds (especially for vegetated areas) (see Posselt et al., 2011a; 2014). In this case, an artificial SEVIRI broadband visible channel that corresponds to MVIRI's broadband visible channel is simulated following the approach of Cros et al. (2006). SEVIRI's two narrow band visible channel (0.6 μm and 0.8 μm) and MVIRI's broadband channel spectral characteristics are used to establish a simple linear model. This model is afterwards applied to SEVIRI's 0.6 μm and 0.8 μm radiance measurements to calculate the broadband visible channel radiance (see Posselt et al., 2014 for more details).

The CM SAF SSR satellite-based product is characterized by a threshold accuracy of 15 W/m^2 for monthly mean data and 25 W/m^2 for daily data (Mueller et al., 2011; Posselt et al., 2012; Sanchez-Lorenzo et al., 2013; Posselt et al., 2014). Posselt et al. (2012) evaluated CM SAF SSR data on a daily and monthly basis against ground-based observations from 12 BSRN (Baseline Surface Radiation Network) stations around the world, showing that both daily and monthly CM SAF data are below the target accuracy for ~90% of the stations. Specifically for Europe, Sanchez-Lorenzo et al. (2013) using monthly SSR data from 47 GEBA (Global Energy Balance Archive) ground stations proceeded to a detailed validation of the CM SAF SSR dataset for the period 1983-2005. They found that CM SAF slightly overestimates SSR by 5.2 W/m^2 (4.4% in relative values). Also, the mean absolute bias was found to be 8.2 W/m^2 which is below the accuracy threshold of 15 W/m^2 (10 W/m^2 for the CM SAF retrieval accuracy and 5 W/m^2 for the surface measurements uncertainties). Applying the Standard Normal Homogeneity Test (SNHT) Sanchez-Lorenzo et al. (2013) revealed that the MFG SSR data over Europe can be considered homogeneous for the period 1994-2005. Recently, Posselt et al. (2014) verified the results of the previous two studies by using a combined MFG-MSG SSR dataset spanning from 1983 to 2010. They found that the monthly mean dataset exhibits a mean bias of +3.16 W/m^2 and a mean absolute bias of 8.15 W/m^2 compared to BSRN which is again below the accuracy threshold of CM SAF. Also, the dataset was found to be homogeneous for the period 1994-2010 in most of the investigated regions except for Africa.

1 To investigate the differences appearing between the RegCM4 and CM SAF SSR fields we also

2 use CFC, COT and Re CM SAF observations from MSG satellites for the period 2004-2009. A

3 description of this cloud optical properties product, also known as CLAAS (CLoud property

4 dAtAset using SEVIRI), can be found in Stengel et al. (2014). The MSG NWC software

5 package v2010 is used for the detection of cloudy pixels, the determination of their type

6 (liquid/ice) and their vertical placement (Derrien and Le Gléau, 2005; NWCSAF, 2010). The

7 detection of cloudy pixels is based on a multispectral threshold method incorporating

8 parameters such us illumination (e.g. daytime, twilight, night-time, sunglint) and type of

9 surface. According to Kniffka et al. (2014), the CM SAF Cloud Mask accuracy is ~90%

10 (successful detection of cloudy pixels for ~90% of the cases) when evaluated against satellite

11 data from CALIOP/CALIPSO and CPR/CloudSat. The bias of the CFC product was found to be

12 2% and 3% for SEVIRI's disk when compared to ground-based data from SYNOP (lidar-radar

13 measurements) and satellite-based data from MODIS, respectively (Stengel et al., 2014). The

14 Cloud Physical Properties (CPP) algorithm (Roebeling et al., 2006; Meirink et al., 2013) is used

15 to retrieve COT at 0.6 μm, Re and CWP. The algorithm is based on the use of SEVIRI's

16 spectral measurements at the visible (0.64 μm) and near infrared (1.63 μm) (Nakajima and

17 King, 1990). First, COT and Re are retrieved for the cloudy pixels and then CWP is given by

18 the following equation:

19

20 $CWP_{ph} = 2/3\ \rho_{ph}\ Re_{ph}\ COT_{ph}$ (8)

21

22 where ph stands for the clouds' phase (liquid/ice) and ρ is the density of water. According to

23 Stengel et al. (2014), the CM SAF COT bias was estimated at -9.9% compared to MODIS

24 observations. The corresponding bias for CWP is -0.3% for liquid phase clouds and -6.2% for

25 ice phase clouds. COT and CWP data are available from CM SAF at a spatial resolution of

26 0.05^{o} x 0.05^{o} on a daily basis. In this work, Re values were calculated from the COT and CWP

27 CM SAF available data using Eq. (8).

28 **2.3 Other data**

29 In addition to the CM SAF SSR and cloud optical properties data used for the evaluation of

30 RegCM4, we also use ancillary data from other sources, namely, AOD, ASY and SSA at 550

31 nm monthly climatological values from the MACv1 climatology (Kinne et al., 2013), monthly

climatological broadband surface shortwave fluxes retrieved from CERES sensors aboard EOS TERRA and AQUA satellites for a 14-year period starting from 3/2000 (Kato et al., 2013) and finally monthly mean total column WV data from ECMWF's ERA-Interim reanalysis (Dee et al., 2011) for the period 2006-2009. All the data were obtained at a spatial resolution of 1° x 1°. It has to be highlighted that these data are similar to the ones used as input within the MAGIC clear sky radiative transfer code (Mueller et al., 2009) which is used for the calculation of CM SAF SSR. Therefore, they can be used in order to examine the reasons for possible deviations appearing between RegCM4 and CM SAF SSR (see Sect. 2.4.). To our knowledge, the uncertainty of the MACv1 aerosol parameters used here has not been reported somewhere in detail. The CERES broadband surface albedo over land exhibits a relative bias of -2.4% compared to MODIS. Specifically, over deserts, the relative bias drops to -2.1% (Rutan et al., 2009). A detailed evaluation of the ERA-Interim WV total column product does not exist. Only recently, the upper troposphere - lower stratosphere WV data were evaluated against airborne campaign measurements showing a good agreement (30% of the observations were almost perfectly represented by the model) (Kunz et al., 2014).

2.4 Methodology

In this study, first, the RegCM4 SSR fields are evaluated against SSR fields from CM SAF (MFG for 2000-2005 and MSG for 2006-2009) for the European region (box region in Fig. S1). Prior to the evaluation, the model and satellite data are averaged on a monthly basis and brought to a common 0.5^o x 0.5^o spatial resolution. It has to be mentioned that the same temporal and spatial resolution was used for all the data utilized in this study. Maps with the normalized mean bias (NMB) (hereafter denoted as bias) are produced on an annual and seasonal basis. NMB is given by the following equation:

$$NMB = \frac{\sum_{i=1}^{N}(\mathrm{Re}\,gCM_i - CMSAF_i)}{\sum_{i=1}^{N} CMSAF_i} 100\% = (\frac{\overline{\mathrm{Re}\,gCM}}{\overline{CMSAF}} - 1)100\% \tag{9}$$

1 where RegCM$_i$ and CMSAF$_i$ represent the RegCM4 and CM SAF mean values for each month

2 i, N is the number of months and $\overline{\mathrm{Re}\,gCM}$, $\overline{CMSAF}$ are the RegCM4 and CM SAF mean

3 values. The statistical significance of the results at the 95% confidence level is checked by

4 means of a two independent sample t-test:

5

6 $$t = (\overline{\mathrm{Re}\,gCM} - \overline{CMSAF}) / \sqrt{(\sigma_{\mathrm{Re}\,gCM}^2 + \sigma_{CMSAF}^2) / N} \qquad (10)$$

7

8 where σ_{RegCM} and σ_{CMSAF} are the standard deviations of RegCM4 and CM SAF total means.

9 When |t| is greater than a critical value that depends on the degrees of freedom (here 2n-1) the

10 bias is considered statistically significant. In addition to the whole European region (EU), the

11 land covered (LA) and ocean covered (OC) part of Europe, seven other sub-regions are

12 defined for the generalization of our results: Northern Europe (NE), Central Europe (CE),

13 Eastern Europe (EE), Iberian Peninsula (IP), Central Mediterranean (CM), Eastern

14 Mediterranean (EM) and Northern Africa (NA) (see Figs. 1a and S1). The bias on an annual

15 and seasonal basis is calculated per region. Apart from bias, other statistical metrics

16 (correlation coefficient R, normalized standard deviation NSD, modified normalized mean

17 bias MNMB, root mean square error RMSE) are also defined, calculated and presented in the

18 Supplement of this manuscript. Specifically for the SSR results presented in the manuscript

19 the Normalized Mean Error (NME) is calculated along with the bias in order to get an insight

20 into the absolute bias between the model simulations and the satellite observations.

21

22 $$NME = \frac{\sum_{i=1}^{N} \left| \mathrm{Re}\,gCM_i - CMSAF_i \right|}{\sum_{i=1}^{N} CMSAF_i} 100\% \qquad (11)$$

23

24 The latitudinal variability of model and satellite-based SSR and their difference is examined by

25 means of seasonal plots. Finally, the seasonal variability of SSR from RegCM4 and CM SAF

26 and their differences is investigated for each of the 10 regions mentioned above. While NMB is

27 primarily used in this work for the investigation of the spatiotemporal variability of RegCM4-

CM SAF deviations, the real difference is given in the plots with the latitudinal and seasonal variability for each region in order to get an insight into the performance of the model, regardless of the SSR levels. The same procedure is done separately for MFG data (2000-2005) and MSG data (2006-2009) to see if the two datasets lead to similar results. Our results are mostly focused on MSG satellite-based observations, since CFC and cloud optical properties data are only available from MSG SEVIRI.

In order to interpret the observed differences between RegCM4 and CM SAF SSR, the same detailed procedure is repeated for CFC and COT for the period 2004-2009. CFC and COT are the two major determinants of the transmission of shortwave radiation through clouds (Gupta et al., 1993) and along with AOD constitute the major controllers of SSR (Kawamoto and Hayasaka, 2008). Therefore, we also proceed to a detailed comparison of RegCM4 AOD at 550 nm (AOD_{550}) against MACv1 climatological data. However, other cloud (Re) and aerosol (ASY, SSA) related parameters also play a significant role. Here, RegCM4 Re is evaluated against observational data from CM SAF while RegCM4 ASY and SSA are compared against climatological data from MACv1 (see Supplement). Specifically, the comparison of RegCM4 data with MACv1 does not constitute an evaluation of the RegCM4 aerosol-related parameters, like in the case of the cloud-related parameters above, since, MACv1 data (Kinne et al., 2013) are climatological (based on a combination of models and observations) and not pure observational data. However, a similar climatology (Kinne et al., 2006) is used for the production of CM SAF SSR (Trentmann et al., 2013). In addition, Mueller et al. (2014) showed that the use of MACv1 aerosol climatology instead of the Kinne et al. (2006) climatology does not affect significantly the CM SAF SSR product. Hence, this comparison allows us to reach useful conclusions about the effect of aerosol representation within RegCM4 on the simulated SSR fields by the model. The same stands for the comparison of RegCM4 ALB data with climatological data from CERES satellite sensors and RegCM4 WV data with WV data from ERA-Interim reanalysis (see Supplement). The CERES ALB 14-year climatology is temporally constant, similar to the CERES climatology used for the production of CM SAF SSR (Trentmann et al., 2013). Finally, the ERA-Interim WV data used here are the same with the WV data incorporated by the radiative scheme of CM SAF. Unlike the RegCM4 evaluation results, the comparison results discussed in this paragraph are presented in the Supplement.

Apart from a qualitative approach, we also proceed to a quantitative study of the reasons that could potentially lead to deviations between the RegCM4 and CM SAF SSR. Using data from

1 RegCM4 and CM SAF and the Santa Barbara DISORT Atmospheric Radiative Transfer

2 (SBDART) model (Ricchiazzi et al., 1998), we estimate the potential relative contribution of the

3 parameters CFC, COT, Re, AOD, ASY, SSA, ALB and WV to the percent RegCM4-CM SAF

4 SSR difference (ΔSSR), over the 7 sub-regions mentioned above. ΔSSR is given by Eq. (11),

5 expressing the percentage of SSR deviation caused by the observed difference between

6 RegCM4 and CM SAF for each parameter (p). First, a SBDART simulation is implemented

7 with a 3-hour timestep for the 15th day of each month (Ming et al., 2005) using monthly mean

8 RegCM4 data as input (control run) for each region. The average of all the timesteps per month

9 expresses the monthly SSR flux (SSR$_{control}$). The SSR fields simulated with SBDART are

10 almost identical to the RegCM4 SSR fields. This indicates that SBDART indeed can be used to

11 study the sensitivity of RegCM4's radiative scheme to various parameters. Then, several

12 SBDART simulations are implemented in the same way, replacing each time only one of the

13 aforementioned input parameters with corresponding values from CM SAF, MACv1 or ERA-

14 Interim (SSR(p)). SSR$_{control}$ and SSR(p) are then used in Eq. (11) to calculate ΔSSR for each

15 month (i) and parameter (p).

16

17 $$\Delta SSR^i(p) = 100(SSR^i_{control} - SSR^i(p))/SSR^i_{control}$$ (11)

18

19 The results of this analysis are presented by means of bar plots for each sub-region. The

20 procedure described above was repeated assuming the simulated SSR fields with all the CM

21 SAF, MACv1 and ERA-Interim input data as the control run and replacing each time the

22 corresponding parameter with data from RegCM4. This was done in order to make sure that the

23 interdependence (the effect of changing a parameter is different under different conditions) of

24 the examined parameters does not impact the validity of our results. In addition, a method like

25 the one introduced by Kawamoto and Hayasaka (2008, 2010, 2011), which is based on the

26 calculation of the sensitivities of SSR on CFC, COT, AOD and WV, was also implemented with

27 similar results (not shown here).

28

3   Results and Discussion

3.1   Surface Solar Radiation

As discussed above, first, we examine the CM SAF and RegCM4 bias patterns for the MFG (2000-2005) and MSG (2006-2009) periods, separately. This work focuses on the MSG dataset, since, cloud properties data which are used in order to investigate the reasons of the observed bias between CM SAF and RegCM4 at a later stage, are only available from MSG. However, we investigate both the periods to examine if the observed biases are valid for the whole simulation period and ensure that there are no differences when using the one or the other dataset. As shown in Fig. S2a and b, the annual bias patterns are similar for both MFG-RegCM4 and MSG-RegCM4. The main feature is a low negative bias over land and a low positive bias over ocean. Overall, the RegCM4 simulations slightly overestimate SSR compared to CM SAF over Europe with a bias of +1.5% in the case of MFG and +3.3% in the case of MSG, while SSR from RegCM4 is much closer to SSR from CM SAF over land (bias of -1.6% for MFG and +0.7% for MSG) than over ocean (bias of +7.2% for MFG and +8.1% for MSG). These values can be found in Table 2 for the RegCM4-MSG period along with the corresponding values for the 7 sub-regions of interest appearing in Fig. 1a while the same values for the RegCM4-MFG period can be found in Table S1 of the Supplement. It has to be highlighted, that hereafter, only results for the MSG CM SAF SSR dataset are presented within the paper while the results for the MFG dataset are included in the Supplement (Figs. S3 to S5).

As presented in Fig. 1, some differences appear in the seasonal bias patterns. A strong positive bias is observed during winter over Northern Europe. For the rest of the regions the winter patterns are very close to the spring and the annual patterns. Contrary to the annual patterns, in summer, the positive bias extends over Europe until the latitudinal zone of $50^{\circ}N$, while in autumn the bias patterns are pretty similar with the annual ones. In winter, the RegCM4 simulations overestimate SSR compared to CM SAF for the whole European domain, the bias being +3.9%. Over land the bias is nearly zero (+0.1%) while over ocean there is a significant bias of +11.3%. As shown in Fig. 1a, NE is by far the sub-region with the strongest bias (+52.4%). Also, NME is 11.4% for the whole European domain (12.0% over land and 10.6% over ocean), EE and NA being the regions with the highest (19.1%) and lowest (7.1%) value, correspondingly (Table 2). The seasonal and annual model and satellite-derived values with the corresponding biases and NMEs and their statistical significance at

the 95% confidence level according to a two independent sample t-test appear in Table 2. The latitudinal variability of RegCM4 SSR, CM SAF SSR and their difference is presented in Fig. 2a. As mentioned in Sect. 2.4, the differences given in the figures with the latitudinal and the seasonal variability are not normalized by the average SSR levels of each region and hence should not be confused with the bias values appearing in the text. For example, while the RegCM4-CM SAF difference is ~7 W/m^2 over NE in winter (comparable to other regions), a strong bias of ~52% characterizes this region due to the low insolation levels at these latitudes. Overall, RegCM4 slightly overestimates SSR at latitudes lower than ~40°N, then a negligible difference between RegCM4 and CM SAF is observed until the latitudinal zone of ~52°N, while, a significant difference is observed for higher latitudes. In spring, a zero bias is observed between the model and CM SAF for Europe. When discriminating between land and ocean covered regions a negative bias is observed over land (-2.9%) and a positive over ocean (+5.2%). The regions with the highest negative bias are NE (-14.2%), EE (-13.5%) and CE (-9.1%), while the regions with the highest positive bias are NA (+8.4%), CM (+7.9%) and EM (+6.7%) (see Table 2). This is also reflected in Fig. 2b where RegCM4 clearly overestimates SSR for latitudes less than ~44°N, significantly underestimating SSR thereafter. NME is 11.4% for the whole European domain, being 12.3% over land and 10.0% over ocean. NME ranges from 5.9% (NA) to 19.8% (NE) (Table 2). In summer, a positive bias of +6.2% is calculated for the whole European domain, the bias being +4.4% over land and +9.4% over ocean. As seen in Table 2, the bias is positive for all the sub-regions ranging from +2.3% (EE) to +10.4% (CM) except for NE (-9.4%). RegCM4 clearly overestimates SSR for latitudes less than ~55°N and underestimates SSR for higher latitudes (Fig. 2c). For the whole European domain NME is 11.1% (10.2% over land and 12.7% over ocean) ranging from 8.0% (EM) to 13.7% (NE) (Table 2). A positive bias of +2.4% is found for Europe in autumn with the corresponding values being -0.9% over land and +8.4% over ocean covered regions. EE (-9.8%) and CE (-7.2%) are the regions with the strongest negative bias while the regions with the strongest positive bias are the ones at the south, namely, NA (+5.5%), CM (+5.3%) and EM (+5.0) (see also Table 2). This is also seen in Fig. 2d where RegCM4 overestimates SSR for latitudes less than ~42°N. NME is 10.5% for the whole European domain being 11.1% over land and 9.3% over ocean. NME ranges from 6.4% (NA) to 17.7% (NE) (Table 2).

The seasonal variability of RegCM4 SSR, CM SAF SSR and their difference for the whole European domain, for the land and ocean covered part of Europe as well as for the 7 sub-regions of interest are presented in Figs. 3a-j. For Europe as a whole, the largest difference

1 between RegCM4 and CM SAF SSR is observed in summer, July being the month with the

2 highest RegCM4-CM SAF difference (20.3 W/m^2). Over land, the difference between

3 RegCM4 and CM SAF SSR is nearly zero for winter and autumn months. During spring, in

4 March and April, RegCM4 underestimates SSR while in summer SSR is overestimated,

5 especially in July. On the contrary, over ocean, SSR is overestimated by RegCM4 for the total

6 of the months. The highest RegCM4-CM SAF differences are observed during the warm

7 period (May-September). Over NE, RegCM4 underestimates SSR for the months from March

8 to September and overestimates SSR during the winter months. The seasonal variability of the

9 difference between RegCM4 and CM SAF is pretty similar over CE and EE. The simulations

10 underestimate SSR in spring (especially during April) and autumn and overestimate SSR in

11 summer. Over IP, SSR is overestimated again in May and during the summer and

12 underestimated in February, March, November and December. For CM and EM, the seasonal

13 variability of the difference between RegCM4 and CM SAF is almost identical. RegCM4

14 significantly overestimates SSR from April to October while for the rest of the months the

15 difference is nearly zero. Finally, over NA, the seasonal variability of the difference is close

16 to the one appearing over CM and EM, but here, SSR is overestimated by RegCM4 also in

17 March.

18 **3.2 Cloud Fractional Cover**

19 CFC plays a determinant role as far as SSR levels are concerned. Therefore, we compare the

20 CFC patterns simulated with RegCM4 against CFC patterns from MSG CM SAF for the

21 common period 2004-2009. Overall, CFC is underestimated by RegCM4 over Europe by

22 24.3% on annual basis (13.7% over land and 38.4% over ocean) despite the fact that over

23 specific regions (e.g. within IP and NA) CFC is overestimated (see Table 3). Underestimation

24 is observed for the total of the four seasons, NA being the only region with a bias of +8.1% in

25 winter and a bias of +13.1% in autumn (see Table S3). As shown in Figs. 4a-d, the

26 underestimation of CFC from RegCM4 is stronger over ocean especially in summer, while

27 strong overestimation is observed over regions in western NA in winter and spring, eastern

28 NA in summer and the whole NA during autumn. The latitudinal variability of RegCM4 CFC,

29 CM SAF CFC and their difference is presented in Fig. 5. A clear, strong underestimation of

30 CFC from RegCM4 is observed for all the latitudinal bands and seasons apart from latitudes

31 around 30° N where CFC is slightly overestimated in autumn. The seasonal variability of

32 RegCM4 CFC, CM SAF CFC and their difference for the whole European domain, for the

1 land and ocean covered part of Europe and for the 7 sub-regions of interest are presented in

2 Figs. 6a-j. CFC is underestimated steadily by RegCM4 throughout a year, the underestimation

3 being much stronger over the ocean than over land (see Figs. 6b and c). This underestimation

4 is observed for all the sub-regions except for NA where CFC is underestimated from April to

5 September and overestimated for the rest of the months.

6 Generally, lower CFCs would lead to higher SSR levels. However, a comparison of the SSR

7 bias patterns appearing in Figs. 1a-d with the CFC bias patterns appearing in Figs. 4a-d and

8 also of the biases appearing in Table 1 and Table S3 and the differences and other metrics

9 appearing in Table S2 and S4 reveals that for some areas and seasons the RegCM4-CM SAF

10 SSR deviations cannot be explained through the corresponding CFC deviations (e.g. land

11 covered regions during spring and autumn). This is in line with the findings of Katragkou et

12 al. (2015) where the WRF-ISCCP SSR deviations could not always be attributed to CFC

13 deviations. As discussed there the role of microphysical cloud properties should also be taken

14 into account. Following this, in the next paragraph we go a step further, taking into account

15 the effect of COT.

3.3 Cloud Microphysical Properties

3.3.1 Cloud Optical Thickness

18 COT is a measure of the transparency of clouds and along with CFC determines the

19 transmission of shortwave radiation through clouds (Gupta et al., 1993). In this paragraph, the

20 RegCM4 COT patterns are compared against COT patterns from MSG CM SAF for the

21 common period 2004-2009. Overall, COT is overestimated by RegCM4 over Europe by 4.3%

22 on annual basis, the bias being positive over land (+7.3%) but negative over ocean (-2.5%)

23 (see Table 3). In addition, COT bias varies with seasons, being positive in spring and autumn

24 and negative in winter and summer (see Tables S5 and S6). As shown in Figs. 7a-d, positive

25 biases are mostly observed over land covered regions of CE, EE and NE and negative biases

26 over NA and the regions around the Mediterranean Sea. In fact, there is a strong latitudinal

27 variability of the RegCM4-CM SAF COT difference for all the seasons as presented in Figs.

28 8a-d. RegCM4 underestimates COT for latitudes below ~45° N in winter, spring and autumn

29 and for latitudes below ~50° N in summer. The seasonal variability of RegCM4 COT, CM

30 SAF COT and their difference for the whole European domain, for the land and ocean

31 covered part of Europe and for the 7 sub-regions of interest are presented in Figs. 9a-j. In

1   general, the RegCM4-CM SAF COT difference is not steadily positive or negative but varies

2   from month to month over both land and ocean. RegCM4 steadily overestimates COT

3   throughout a year only over NE and underestimates COT over CM and NA. It has to be

4   highlighted that there are no COT retrievals over NE for December and January due to a

5   limited illumination at that latitudes during this period of the year. This is also the reason for

6   the missing grid cells appearing in the top-right corner of Figs. 7a-d.

7   A comparison of the SSR bias patterns appearing in Figs. 1a-d with the CFC (Figs. 4a-d) and

8   the COT (Figs. 7a-d) bias patterns reveals that COT could explain part of the RegCM4-CM

9   SAF SSR deviations that could not be explained through CFC (e.g. NE, CE, EE). The same

10 conclusions can be reached by comparing the seasonal variability of SSR, CFC and COT over

11 the region of interest (see Figs. 3, 6 and 9). However, other parameters are expected to be

12 responsible for the remaining unexplained RegCM4-CM SAF SSR deviation.

13 **3.3.2 Cloud Effective Radius**

14 Re is a microphysical optical property expressing the size of cloud droplets in the case of

15 liquid clouds and the size of ice crystals in the case of ice clouds. Re of liquid (Rel) and ice

16 (Rei) clouds plays a critical role in the calculation of the optical thickness of clouds as well as

17 their albedo (see Eqs. 4-7 in Sect. 2.1.). The evaluation of RegCM4 Rel and Rei against

18 observational data from CM SAF reveals a significant underestimation over the whole

19 European domain (bias of -36.1% for Rel and -28.3% for Rei) (see Tables 3, S7 and S8). This

20 is also apparent in the maps appearing in Figs. S6 and S8. In the case of ice clouds, the biases

21 over land and ocean do not differ significantly. On the contrary, for liquid clouds, the bias

22 over land is more than double the bias over ocean (see Tables 3, S7 and S8). This is due to the

23 very low RegCM4 Rel values appearing over land while the CM SAF dataset does not exhibit

24 such a land-ocean difference. A possible explanation for this could be the fact that for liquid

25 clouds a different approach is used over land (constant Rel of 10 μm) and ocean (Eq. 1) while

26 for ice clouds the parameterization is the same for land and ocean (Eq. 2). The fact that the

27 average Rel value over land (5.65±1.06 μm) is very close to the lowest Rel boundary (5 μm)

28 according to Eq. (1), possibly points towards an underestimation of the liquid cloud height

29 and vertical development. Also, this Rel land-ocean difference is in charge of the COT land-

30 ocean difference (see Table 3) according to Eq. (4). In general, the underestimation of Re

31 would result into more reflective clouds and hence into underestimated SSR levels. It has to

32 be mentioned here that the latitudinal and monthly variability of RegCM4 Rel and Rei, CM

1   SAF Rel and Rei and their difference for the whole European domain, for the land and ocean

2   covered part of Europe and for the 7 sub-regions are presented in the Supplement of this

3   manuscript (Figs. S6 to S9). A constant underestimation of Rel and Rei is observed for the

4   whole Europe.

5   3.4   Aerosol Optical Properties

6   As discussed in Sect. 2.4., AOD along with CFC and COT constitute the major controllers of

7   SSR. A comparison of the RegCM4 AOD_{550} seasonal patterns with climatological AOD_{550}

8   values from MACv1 is presented in Figs. S10a-d. On an annual basis, RegCM4 overestimates

9   AOD over the region of NA (bias of +25.0%) (see Table 3). The overestimation is very strong

10   during winter being much weaker in spring and autumn (see Tables S9 and S10). This

11   overestimation over regions affected by dust emission has been discussed comprehensively in

12   Nabat et al. (2012) and has to do with the dust particle size distribution schemes utilized by

13   RegCM4 (Alfaro and Gomes, 2001; Kok, 2011). Nabat et al. (2012) showed that the

14   implementation of Kok (2011) scheme generally returns AODs closer to that of MODIS

15   within the Mediterranean Basin. However, a first climatological comparison of RegCM4 dust

16   AODs with data from CALIOP/CALIPSO (A. Tsikerdekis, personal communication, 2015)

17   has shown that both schemes overestimate dust AOD over Europe and therefore the selection

18   of a specific dust scheme is not expected to change drastically our results. On the contrary,

19   AOD is significantly underestimated over the rest of the domain. This should be expected as

20   RegCM does not account for several types of aerosols, anthropogenic (e.g. nitrates,

21   ammonium and secondary organic aerosols, industrial dust) and natural (e.g. biogenic

22   aerosols) which potentially play an important role (Kanakidou et al., 2005; Zanis et al., 2012).

23   This overestimation/underestimation dipole in winter, spring and autumn is also reflected in

24   Fig. S11. RegCM4 overestimates AOD for latitudes below ~40° N in winter, for latitudes

25   below ~35° N in spring and for a narrow latitudinal band (~30-33° N) in autumn. In summer,

26   RegCM4 steadily underestimates AOD compared to MACv1. The seasonal variability of

27   RegCM4 AOD_{550}, MACv1 AOD_{550} and their difference for the whole European domain, for

28   the land and ocean covered part of Europe and for the 7 sub-regions of interest are presented

29   in Figs. S12a-j. In general, RegCM4 clearly underestimates AOD throughout a year over

30   regions that are not affected heavily by Sahara dust transport. This underestimation would

31   cause an overestimation of SSR if all the other parameters were kept constant. The opposite

32   stands for the region of NA where AOD, except for summer, is significantly overestimated.

1   As in the case of COT and Re, in order to fully assess the contribution of aerosols to the

2   observed RegCM4-CM SAF SSR deviations, one has to take into account ASY and SSA

3   apart from AOD. A comparison of RegCM4 ASY with climatological values from MACv1

4   reveals a small underestimation from RegCM4 over Europe (bias of -1.1%) (Table 3 and

5   S11). As shown in Fig. S13, RegCM4 underestimates ASY for latitudes below ~ 40°N and

6   slightly overestimates ASY for the rest of the region. Except for NA where RegCM4

7   underestimates ASY throughout the year, RegCM4 slightly overestimates ASY for the warm

8   period over NE, CE and EE while for the rest of the sub-regions the RegCM4-MACv1

9   difference is close to zero (see Fig. S14). Contrary to the case of ASY, RegCM4 steadily

10 underestimates SSA compared to MACv1 over Europe by 4.2 % (see Tables 3 and S12 and

11 Fig. S15). Moreover, as shown in Fig. S16, SSA is underestimated on an annual basis for the

12 total of the sub-regions.

13

14 **3.5   Other parameters**

15 Apart from the major (CFC, COT, AOD) and minor (Re, ASY, SSA) SSR determinants

16 which are discussed above in detail, there are also a number of other parameters that could

17 impact the simulation skills of RegCM4 compared to CM SAF, since these parameters are

18 used as input within the radiative scheme of the model.

19 As it was previously discussed, WV is another parameter that affects the transmission of solar

20 radiation within the atmosphere. RegCM4 is found here to overestimate WV compared to

21 ERA-Interim reanalysis all over Europe with a bias of ~12% (see Tables 3 and S13). This

22 becomes more than obvious when looking into the bias map, the seasonal and latitudinal

23 variability of the two datasets (see Figs. S17 and S18).

24 **3.6   In line with the study of Güttler et al. (2014), RegCM4 exhibits a significant**

25 **underestimation of ALB over CE, EE and NA (see Tables 3 and S14)**

26 **compared to climatological data from CERES (see Sect. 2.3.). In general,**

27 **there is a striking difference between land and ocean covered regions**

28 **(see Figs. S19 and S20). Over land RegCM4 underestimates ALB by 28.3%**

29 **while over ocean ALB is strongly overestimated by 131%. As it was**

30 **previously   highlighted,   the   comparisons   of   RegCM4   with   non-**

observational data presented in this paragraph do not constitute an evaluation of RegCM4. However, these comparisons give us an insight into how several parameters affect the ability of RegCM4 to simulate SSR. Assessing the effect of various parameters on RegCM's SSR

As discussed in detail in Sect. 2.4., the potential contribution of each one of the aforementioned parameters in the deviation between RegCM4 and CM SAF SSR is assessed with the use of SBDART radiative transfer model. The results of this analysis are presented in Fig. 10. The percent contribution of each parameter to the RegCM4-CM SAF SSR difference is calculated on a monthly basis. Results for NE are not included in this manuscript, since COT and Re are not available from CM SAF during winter (December, January) and also due to the low insolation levels for several months at high latitudes. Results for NA are also not presented. This region is characterized by a significant day-by-day variability of cloudiness and aerosols and therefore the statistical significance of a monthly analysis like the one presented here would be limited. Another source of uncertainty would be the use of spatial averages within the radiative transfer simulations since the western and eastern part of the region differ significantly by means of aerosol load and cloud coverage and hence the region cannot be considered homogenous.

It has to be highlighted that the potential percent contributions to the RegCM4-CM SAF SSR difference presented in Fig. 10 do not include the relative contribution due to algorithmic issues of the CM SAF product used here and also uncertainties inserted from the method itself (e.g. SBDART simulation accuracy, use of monthly data, spatial averaging, etc.). Therefore the contributions appearing in Fig. 10 are not directly connected to the RegCM4-CM SAF differences presented in Fig. 3. In fact, part of these differences is due to the overestimation of SSR by CM SAF due to the method used for the production of the dataset. Hence, the ΔSSR values presented below do not include the bias inserted by the CM SAF algorithm. As mentioned in Sect. 2.2, CM SAF was found to overestimate SSR compared to ground observations over Europe by 5.2 W/m^2 for the 1983-2005 MFG period (Sanchez-Lorenzo et al., 2013) and by 3.16 W/m^2 for the 1983-2010 MFG-MSG period (Posselt et al., 2014). Following these studies, the CM SAF MSG data (2006-2009) used in this work are validated using ground-based observations from 26 stations (23 stations from the Word Radiation Data Center - WRDC and 3 independent stations) evenly distributed around Europe (see Fig. S21). Overall, it is found that CM SAF overestimates SSR on an annual basis by 4.5 W/m^2 over CE,

1   8.8 W/m^2 over EE, 2.4 W/m^2 over IP, 7.8 W/m^2 over CM and 4.5 W/m^2 over EM, the

2   overestimation being much higher during the warm period (Fig. S22).

3   As seen in Fig. 10a, apart from the bias inserted by the CM SAF retrieval methodology, the

4   percent RegCM4-CM SAF SSR difference (ΔSSR) over CE is mostly determined by CFC,

5   COT and AOD. However, for specific months, Re and the other parameters also play an

6   important role leading to an underestimation of SSR. CFC leads to a significant

7   overestimation of SSR on an annual basis ranging from 3.7% (April) to 18.6% (January).

8   Apart from July, COT leads to an underestimation of SSR, April being the month with the

9   highest underestimation (ΔSSR of -13.3%). AOD on the other hand, leads to an

10   overestimation of SSR over CE ranging from +4.6% (June) to +9.5% (January). As mentioned

11   in Sect. 2.4, the procedure was repeated assuming the simulated SSR fields with all the CM

12   SAF, MACv1 and ERA-Interim input data as the control run and replacing each time the

13   corresponding parameter with data from RegCM4. The results from this repetition were

14   similar with the results presented above showing that the effect of the interdependence of the

15   parameters investigated here is low and does not affect the validity of our results. The same

16   stands for all the sub-regions. The results from the inverse procedure and the differences with

17   the results presented here are given in Figs. S23 and S24, respectively.   In line with CE,

18   ΔSSR over EE is mostly determined by CFC, COT and AOD (Fig. 10b). Apart from April,

19   CFC leads to an overestimation of SSR, December being the month with the highest

20   overestimation (+22.9%). Apart from June and July, COT causes an underestimation of SSR,

21   March/August being the month with the highest/lowest underestimation (-15.8%/-0.2%). On

22   the other hand, AOD leads to an overestimation of SSR the whole year, December/May being

23   the month with the highest/lowest overestimation (+12.3%/+4.2%). Re also plays a role

24   leading to an underestimation of SSR, that ranges from -1.06% (July) to -2.5% (February). All

25   the other parameters play a minor role, generally leading to an underestimation of SSR.

26   Over IP, despite the fact that the dominant parameters are CFC and COT, for some months

27   AOD, SSA and Re contribute substantially in ΔSSR (Fig. 10c). CFC leads to an

28   overestimation of SSR, January/September being the month with the highest/lowest

29   overestimation of SSR (+9.1%/+1.1%). COT causes an important overestimation of SSR from

30   April to October (e.g. +3.7% in June) and a significant underestimation during March (-

31   2.8%). On the other hand, Re leads to an underestimation of SSR that ranges from -1.3% in

32   April to -0.3% in August. The same stands for SSA with an average annual SSR

underestimation of -1.2%, while AOD exhibits a mixed behavior leading to either underestimation (a maximum of -6.1% in December) or overestimation (a maximum of +4.9% in March).

As seen in Fig. 10d, ΔSSR over CM is mostly determined by CFC, COT, AOD and SSA. CFC causes a significant overestimation of SSR ranging from +3.2% (July) to +11.9% (December). COT leads to an overestimation of SSR on an annual basis, October being the month with the highest overestimation (+4.6%). AOD causes an overestimation of SSR over CM for the period from March to October (average ΔSSR of +2.2%) and an underestimation during winter (average ΔSSR of-2.3%). SSA on the other hand, causes an underestimation of SSR on an annual basis ranging from -0.5% (July) to -1.9% (December).

ΔSSR over EM is dominated by the relative contribution of CFC, AOD and COT (see Fig., 10e). CFC causes an overestimation of SSR on an annual basis ranging from +1.7% (August) to +12.2% (December). Apart from February, AOD causes a significant overestimation ranging from +0.5% (March) to +6.0% (September). Apart from March, COT leads to an overestimation of SSR, February being the month with the highest overestimation (+4.3%). SSA also plays a role, in some cases comparable in magnitude to that of COT or AOD (e.g. January, March).

Concluding, for the total of the five sub-regions, CFC, COT and AOD are the most important factors that determine the SSR deviations between RegCM4 and CM SAF on an annual basis. The underestimations/overestimations of CFC, COT and AOD by the model cause an annual absolute deviation of the SSR compared to CM SAF of 8.4%, 3.8% and 4.5%, respectively.

4 Conclusions

In the present study, a decadal simulation (2000-2009) with the regional climate model RegCM4 is implemented in order to assess the model's ability to represent the SSR patterns over Europe. The RegCM4 SSR fields are evaluated against satellite-based observations from CM SAF. The annual bias patterns of RegCM4-CM SAF are similar for both MFG (2000-2005) and MSG (2006-2009) observations. The model slightly overestimates SSR compared to CM SAF over Europe, the bias being +1.5% for MFG and +3.3% for MSG observations. Moreover, the bias is much lower over land than over ocean while some differences appear locally between the seasonal and annual bias patterns.

1   In order to understand the RegCM4-CM SAF SSR deviations, CFC, COT and Re data from

2   RegCM4 are compared against observations from CM SAF (MSG period). For the same

3   reason, AOD, ASY, SSA, WV and ALB from RegCM4 are compared against data from

4   MACv1, ERA-Interim reanalysis and CERES since these data are similar to the ones used as

5   input in the retrieval of CM SAF SSR.

6   CFC is significantly underestimated by RegCM4 compared to CM SAF over Europe by

7   24.3% on annual basis. Part of the bias between REGCM4 and CM SAF SSR can be

8   explained through CFC with the underestimation of CFC leading to a clear overestimation of

9   SSR. It was also found that RegCM4 overestimates COT compared to CM SAF on an annual

10 basis suggesting that COT may explain part of the RegCM4-CM SAF SSR deviations that

11 could not be explained through CFC over specific regions. In addition, RegCM4

12 underestimates significantly Rel and Rei compared to CM SAF over the whole European

13 domain on an annual basis. A comparison of the RegCM4 AOD seasonal patterns with AOD

14 values from the MACv1 aerosol climatology reveals that RegCM4 overestimates AOD over

15 the region of NA and underestimates it for the rest of the European domain. ASY and SSA are

16 slightly underestimated by the model. The comparison of RegCM4 WV against data from

17 ERA-Interim reanalysis reveals a clear overestimation over Europe. In line with previous

18 studies, RegCM4 underestimates ALB significantly over CE, EE and NA compared to

19 climatological data from CERES with a striking difference between land and ocean.

20 The combined use of SBDART radiative transfer model with RegCM4, CM SAF, MACv1,

21 CERES and ERA-Interim data for the common period 2006-2009 shows that the difference

22 between RegCM4 and CM SAF SSR, apart from the bias inserted by the CM SAF algorithm,

23 is mostly explained through CFC, COT and AOD deviations. In the majority of the regions,

24 CFC leads to an overestimation of SSR by RegCM4. In some cases, COT leads to a

25 significant underestimation of SSR by RegCM4, while for the majority of the regions leads to

26 an overestimation. AOD is generally responsible for the overestimation of SSR. The other

27 parameters (Re, ASY, SSA, WV and ALB) play a less significant role, in the RegCM4-CM

28 SAF SSR deviations. Overall, CFC, COT and AOD are the major determinants of the SSR

29 differences between RegCM4 and CM SAF, causing an absolute deviation on an annual basis

30 of 8.4%, 3.8% and 4.5%, respectively. These results highlight the importance of other

31 parameters apart from CFC which was examined in previous model evaluation studies (e.g.

Jaeger et al., 2008; Markovic et al., 2008; Kothe and Ahrens, 2010; Kothe et al., 2011; 2014; Güttler et al., 2014).

Overall, it is shown in this study that RegCM4 simulates adequately the SSR patterns over Europe. However, it is also shown that the model overestimates or underestimates significantly several parameters that determine the transmission of solar radiation in the atmosphere. The good agreement between RegCM4 and satellite-based SSR observations from CM SAF is at a great extent result of the contradicting effect of these parameters. Our results suggest that there should be a reassessment of the way these parameters are represented within the model so that SSR is not only well simulated but also for the right reasons. This would also allow for a safer investigation of the dimming/brightening effect since the SSR deviations would be safely dedicated to the one or the other parameter. It is suggested here that a similar approach should be implemented in the future to the same or other regional climate models with various setups also utilizing new satellite products (e.g. CM SAF SARAH).

Acknowledgements

References

Alfaro, S. C. and Gomes, L.: Modeling mineral aerosol production by wind erosion: Emission intensities and aerosol size distribution in source areas, J. Geophys. Res., 106, 18075-18084, doi:10.1029/2000JD900339, 2001.

Allen, M. R. and Ingram, W. G.: Constraints on future changes in climate and the hydrologic cycle, Nature, 419, 224-232, 2002.

Beyer, H. G., Costanzo, C., and Heinemann, D.: Modifications of the Heliosat procedure for irradiance estimates from satellite images, Solar Energy, 56, 207-212, doi:10.1016/0038-092X(95)00092-6, 1996.

Bodas-Salcedo, A., Williams, K. D., Ringer, M. A., Beau, I., Cole, J. N. S., Dufresne, J.-L., Koshiro, T., Stevens, B., Wang, Z. and Yokohata T.,: Origins of the Solar Radiation Biases over the Southern Ocean in CFMIP2 Models, J. Climate, 27, 41–56, doi:10.1175/JCLI-D-13-00169.1, 2014

Briegleb, B. P.: Delta-Eddington approximation for solar radiation in the NCAR Community Climate Model, J. Geophys. Res., 97, 7603-7612, doi:10.1029/92JD00291, 1992.

Cano, D., Monget, J., Albuisson, M., Guillard, H., Regas, N., and Wald, L.: A method for the determination of the global solar radiation from meteorological satellite data, Sol. Energy, 37, 31-39, doi:10.1016/0038-092X(86)90104-0, 1986.

Chiacchio, M., Solmon, F., Giorgi, P. Stackhouse, and Wild, M.: Evaluation of the radiation budget with a regional climate model over Europe and inspection of dimming and brightening, J. Geophys. Res., 120, doi:10.1002/2014JD022497, 2015.

Collins, W. D., Bitz, C. M., Blackmon, M. L., Bonan, G. B., Bretherton, C. S., Carton, J. A., Chang, P., Doney, S. C., Hack, J. J., Henderson, T. B., Kiehl, J. T., Large, W. G., McKenna, D. S., Santer, B. D., and Smith, R. D.: The Community Climate System Model version 3 (CCSM3), J. Climate, 19, 2122-2143, doi:10.1175/JCLI3761.1, 2006.

Cros, S., Albuisson, M., and Wald, L.: Simulating Meteosat-7 broadband radiances using two visible channels of Meteosat-8, Solar Energy, 80, 361-367, doi:10.1016/j.solener.2005.01.012, 2006.

Dee, D. P., Uppala, S. M., Simmons, A. J., Berrisford, P., Poli,P., Kobayashi, S., Andrae, U., Balmaseda, M. A., Balsamo, G., Bauer, P., Bechtold, P., Beljaars, A. C. M., van de Berg, L.,

1 Bidlot, J., Bormann, N., Delsol, C., Dragani, R., Fuentes, M., Geer, A. J., Haimberger, L.,
2 Healy, S. B., Hersbach, H., Hólm, E. V., Isaksen, L., Kållberg, P., Köhler, M., Matricardi, M.,
3 McNally, A. P., Monge-Sanz, B. M., Morcrette, J.-J., Park, B.-K., Peubey, C., de Rosnay, P.,
4 Tavolato, C., Thépaut, J.-N., and Vitart, F.: The ERA-Interim reanalysis: configuration and
5 performance of the data assimilation system, Q. J. Roy. Meteor. Soc., 137, 553-597,
6 doi:10.1002/qj.828, 2011.

7 Derrien, M. and Le Gléau, H.: MSG/SEVIRI cloud mask and type from SAFNWC, Int. J.
8 Remote Sens., 26, 4707–4732, 2005.

9 Dickinson, R. E., Henderson-Sellers, A., and Kennedy, P. J.: Biosphere-atmosphere transfer
10 scheme (bats) version 1e as coupled to the NCAR community climate model, Tech. Rep.
11 NCAR/TN-387+STR, National Center for Atmospheric Research, Boulder, Colorado, USA,
12 1-72, doi:10.5065/D67W6959, 1993.

13 Emanuel, K. A. and Zivkovic-Rothman, M.: Development and evaluation of a convection
14 scheme for use in climate models, J. Atmos. Sci., 56, 1766-1782, 1999.

15 Emanuel, K. A.: A scheme for representing cumulus convection in large-scale models, J.
16 Atmos. Sci., 48, 2313-2335, 1991.

17 Flato, G., Marotzke, J., Abiodun, B., Braconnot, P., Chou, S., Collins, W., Cox, P., Driouech,
18 F., Emori, S., Eyring, V., Forest, C., Gleckler, P., Guilyardi, E., Jakob, C., Kattsov, V.,
19 Reason, C., and Rummukainen, M.: Evaluation of climate models, in: Climate Change 2013:
20 The Physical Science Basis. Contribution of Working Group I to the Fifth Assess- ment
21 Report of the Intergovernmental Panel on Climate Change, edited by Stocker, T., Qin, D.,
22 Plattner, G.-K., Tignor, M., Allen, S., Boschung, J., Nauels, A., Xia, Y., Bex, V., and
23 Midgley, P., chap. 6, 741-866, Cambridge University Press, Cambridge, United Kingdom and
24 New York, NY, USA, 2013.

25 Giorgi, F., Coppola, E., Solmon, F., Mariotti, L., Sylla, M. B., Bi, X., Elguindi, N., Diro, G.
26 T., Nair, V., Giuliani, G., Cozzini, S., Guettler, I., O'Brien, T. A., Tawfik, A. B., Shalaby, A.,
27 Zakey, A. S., Steiner, A. L., Stordal, F., Sloan, L. C., and Brankovic, C.: RegCM4: model
28 description and preliminary tests over multiple CORDEX domains, Clim. Res., 52, 7-29,
29 doi:10.3354/cr01018, 2012.

1 Grell, G. A., Dudhia, J., and Stauffer, D. R.: Description of the fifth generation Penn
2 State/NCAR Mesoscale Model (MM5), Tech. Rep. NCAR/TN-398+STR, National Center for
3 Atmospheric Research, Boulder, Colorado, USA, 1-121, doi:10.5065/D60Z716B, 1994.

4 Grell, G.: Prognostic evaluation of assumptions used by cumulus parameterizations, Mon.
5 Wea. Rev., 121, 764-787, 1993.

6 Gu, L., Baldocchi, D., Verma, S., Black, T., Vesala, T., Falge, E., and Dowty, P.: Advantages
7 of diffuse radiation for terrestrial ecosystem productivity, J. Geophys. Res., 107(D6), 4050,
8 doi:10.1029/2001JD001242, 2002.

9 Gupta, S. K., Staylor, W. F. , Darnell, W. L., Wilber, A. C., and Ritchey, N. A.: Seasonal
10 variation of surface and atmospheric cloud radiative forcing over the globe derived from
11 satellite data, J. Geophys. Res., 98(D11), 20761-20778, doi:10.1029/93JD01533, 1993.

12 Güttler I, Branković, Č., Srnec, L., Patarčić, M.: The impact of boundary forcing on
13 RegCM4.2 surface energy budget, Climatic Change, 125, 67-78, doi:10.1007/s10584-013-
14 0995-x, 2014

15 Hammer, A., Heinemann, D., Hoyer, C. R. K., Lorenz, E., Mueller, R., and Beyer, H.: Solar
16 energy assessment using remote sensing technologies, Remote Sens. Environ., 86, 423-432,
17 doi:10.1016/S0034-4257(03)00083-X, 2003.

18 Holtslag, A. A. M., De Bruijn, E. I. F., and Pan, H.-L.: A High Resolution Air Mass
19 Transformation Model for Short-Range Weather Forecasting, Mon. Weather Rev., 118, 1561-
20 1575, 1990.

21 IPCC: Climate Change 2013: The Physical Science Basis: Summary for Policymakers,
22 Cambridge University Press, Cambridge, United Kingdom and New York, NY, USA, 2013.

23 Jaeger, E. B., Anders, I., Lüthi, D., Rockel, B., Schär, C., and Seneviratne, S. I.: Analysis of
24 ERA40-driven CLM simulations for Europe, Meteorol. Z., 17(4), 349-367, 2008.

25 Kanakidou, M., Seinfeld, J. H., Pandis, S. N., Barnes, I., Dentener, F. J., Facchini, M. C., Van
26 Dingenen, R., Ervens, B., Nenes, A., Nielsen, C. J., Swietlicki, E., Putaud, J. P., Balkanski,
27 Y., Fuzzi, S., Horth, J., Moortgat, G. K., Winterhalter, R., Myhre, C. E. L., Tsigaridis, K.,
28 Vignati, E., Stephanou, E. G., and Wilson, J.: Organic aerosol and global climate modelling: a
29 review, Atmos. Chem. Phys., 5, 1053-1123, doi:10.5194/acp-5-1053-2005, 2005.

1   Kato, S., Loeb, N. G., Rose, F. G., Doelling, D. R., Rutan, D. A., Caldwell, T. E., Yu, L., and
2   Weller, R. A.: Surface Irradiances Consistent with CERES-Derived Top-of-atmosphere
3   Shortwave and Longwave Irradiances, J. Climate, 26, 2719-2740, doi:10.1175/JCLI-D-12-
4   00436.1, 2013.

5   Katragkou, E., García-Díez, M., Vautard, R., Sobolowski, S., Zanis, P., Alexandri, G.,
6   Cardoso, R. M., Colette, A., Fernandez, J., Gobiet, A., Goergen, K., Karacostas, T., Knist, S.,
7   Mayer, S., Soares, P. M. M., Pytharoulis, I., Tegoulias, I., Tsikerdekis, A., and Jacob, D.:
8   Regional climate hindcast simulations within EURO-CORDEX: evaluation of a WRF multi-
9   physics ensemble, Geosci. Model Dev., 8, 603-618, doi:10.5194/gmd-8-603-2015, 2015.

10   Kawamoto, K. and Hayasaka, T.: Cloud and aerosol contributions to variation in shortwave
11   surface irradiance over East Asia in July during 2001 and 2007, J. Quant. Spectros. Radiat.
12   Transfer, 112, 329-337, doi:10.1016/j.jqsrt.2010.08.002, 2012.

13   Kawamoto, K. and Hayasaka, T.: Geographical features of changes in surface shortwave
14   irradiance in East Asia estimated using the potential radiative forcing index, Atmos. Res., 96,
15   337-343, doi:10.1016/j.atmosres.2009.09.016, 2010.

16   Kawamoto, K. and Hayasaka, T.: Relative contributions to surface shortwave irradiance over
17   China: A new index of potential radiative forcing, Geophys. Res. Lett., 35, L17809,
18   doi:10.1029/2008GL035083, 2008.

19   Kiehl, J. T., Hack, J. J., Bonan, G. B., Boville, B. A., Breigleb, B. P., Williamson, D., and
20   Rasch, P.: Description of the NCAR community climate model (CCM3), Tech. Rep.
21   NCAR/TN-420+STR, National Center for Atmospheric Research, Boulder, Colorado, USA,
22   1-159, doi:10.5065/D6FF3Q99, 1996.

23   Kiehl, J. T., Hack, J. J., Bonan, G. B., Boville, B. B., Williamson, D. L., and Rasch, P. J.: The
24   National Center for Atmospheric Research Community Climate Model: CM3, J. Climate, 11,
25   1131-1149, 1998.

26   Kim, D. and Ramanathan, V.: Solar radiation budget and radiative forcing due to aerosols and
27   clouds, J. Geophys. Res., 113, D02203, doi:10.1029/2007JD008434, 2008.

28   Kinne, S., et al.: An AeroCom initial assessment-optical properties in aerosol component
29   modules of global models, Atmos. Chem. Phys., 6, 1815-1834, doi:10.5194/acp-6-1815-2006,
30   2006.

1 Kinne, S., O'Donnel, D., Stier, P., Kloster, S., Zhang, K., Schmidt, H., Rast, S., Giorgetta, M.,

2 Eck, T. F., and Stevens, B.: MACv1: A new global aerosol climatology for climate studies, J.

3 Adv. Model. Earth Syst., 5, 704–740, 2013.

4 Kniffka, A., Stengel, M., and Hollmann, R.: Validation Report, SEVIRI cloud mask data set,

5 Satellite Application Facility on Climate Monitoring, 21 pp.,

6 doi:10.5676/EUM_SAF_CM/CMA_SEVIRI/V001, 2014.

7 Kniffka, A., Stengel, M., and Hollmann, R.: Validation Report, SEVIRI cloud mask data set,

8 Satellite Application Facility on Climate Monitoring, 21 pp., available at: www.cmsaf.eu,

9 doi:10.5676/EUM_SAF_CM/CMA_SEVIRI/V001, 2014.

10 Kok, J. F.: A scaling theory for the size distribution of emitted dust aerosols suggests climate

11 models underestimate the size of the global dust cycle, P. Natl. Acad. Sci. USA, 108, 1016-

12 1021, doi:10.1073/pnas.1014798108, 2011.

13 Kothe, S. and Ahrens, B.: On the radiation budget in regional climate simulations for West

14 Africa, J. Geophys. Res., 115, D23120, doi:10.1029/2010JD014331, 2010.

15 Kothe, S., Dobler, A., Beck, A., and Ahrens, B.: The radiation budget in a regional climate

16 model, Climate Dynam. 36, 1023-1036, doi:10.1007/s00382-009-0733-2, 2011.

17 Kothe, S., Panitz, H.-J., and Ahrens, B.: Analysis of the radiation budget in regional climate

18 simulations with COSMO-CLM for Africa, Met. Z., 23, 123-141 doi:10.1127/0941-

19 2948/2014/0527, 2014.

20 Kotlarski, S., Keuler, K., Christensen, O. B., Colette, A., Déqué, M., Gobiet, A., Goergen, K.,

21 Jacob, D., Lüthi, D., van Meijgaard, E., Nikulin, G., Schär, C., Teichmann, C., Vautard, R.,

22 Warrach-Sagi, K., and Wulfmeyer, V.: Regional climate modeling on European scales: a joint

23 standard evaluation of the EUROCORDEX RCM ensemble, Geosci. Model Dev., 7, 1297-

24 1333, doi:10.5194/gmd-7-1297-2014, 2014.

25 Kunz, A., Spelten, N., Konopka, P., Müller, R., Forbes, R. M., and Wernli, H.: Comparison of

26 Fast In situ Stratospheric Hygrometer (FISH) measurements of water vapor in the upper

27 troposphere and lower stratosphere (UTLS) with ECMWF (re)analysis data, Atmos. Chem.

28 Phys., 14, 10803-10822, doi:10.5194/acp-14-10803-2014, 2014.

1   Lamarque, J.-F., et al.: Historical (1850–2000) gridded anthropogenic and biomass burning
2   emissions of reactive gases and aerosols: methodology and application, Atmos. Chem. Phys.,
3   10, 7017-7039, doi:10.5194/acp-10-7017-2010, 2010.

4   Laprise, R.: Regional climate modelling, J. Comput. Phys., 227, 3641-3666, 2008.

5   Markovic, M., Jones, C. G., Vaillancourt, P. A., Paquin, D., Winger, K., and Paquin-Ricard,
6   D.: An evaluation of the surface radiation budget over North America for a suite of regional
7   climate models against surface station observations, Clim. Dyn., 31, 779-794,
8   doi:10.1007/s00382-008-0378-6, 2008.

9   Meirink, J. F., Roebeling, R. A., and Stammes, P.: Inter-calibration of polar imager solar
10 channels using SEVIRI, Atmos. Meas. Tech., 6, 2495-2508, doi:10.5194/amt-6-2495-2013,
11 2013.

12 Mercado, L. M., Bellouin, N., Sitch, S., Boucher, O., Huntingford, C., Wild, M., and Cox, P.
13 M.: Impact of changes in diffuse radiation on the global land carbon sink, Nature, 458, 1014-
14 1017, doi:10.1038/nature07949, 2009.

15 Ming, Y., Ramaswamy, V., Ginoux, P. A., and Horowitz, L. H.: Direct radiative forcing of
16 anthropogenic organic aerosol, J. Geophys. Res., 110, D20208, doi:10.1029/2004JD005573,
17 2005.

18 Mueller, R., Matsoukas, C., Gratzki, A., Hollmann, R., Behr, H.: The CM-SAF operational
19 scheme for the satellite based retrieval of solar surface irradiance-a LUT based eigenvector
20 hybrid approach, Remote Sens. Environ., 113, 1012-1022, doi:10.1016/j.rse.2009.01.012,
21 2009.

22 Mueller, R., Träger-Chatterjee, C.: Brief Accuracy Assessment of Aerosol Climatologies for
23 the Retrieval of Solar Surface Radiation, Atmosphere, 5, 959-972,
24 doi:10.3390/atmos5040959, 2014.

25 Mueller, R., Trentmann, J., Träger-Chatterjee, C., Posselt, R., Stöckli, R.: The role of the
26 effective cloud Albedo for climate monitoring and analysis, Remote Sens., 3, 2305-2320,
27 doi:10.3390/rs3112305, 2011.

28 Nabat, P., Solmon, F., Mallet, M., Kok, J. F., and Somot, S.: Dust emission size distribution
29 impact on aerosol budget and radiative forcing over the Mediterranean region: a regional

climate model approach, Atmos. Chem. Phys., 12, 10545-10567, doi:10.5194/acp-12-10545 2012, 2012.

Nakajima, T. and King, M. D.: Determination of the optical thickness and effective particle radius of clouds from reflected solar radiation measurements, Part 1: Theory, J. Atmos. Sci., 47, 1878-1893, 1990.

NWCSAF: Algorithm Theoretical Basis Document for "Cloud Products" (CMa-PGE01 v3.0, CT-PGE02 v2.0 & CTTH-PGE03 v2.1), EUMETSAT Satellite Application Facility on Nowcasting and Shortrange Forecasting, SAF/NWC/CDOP/MFL/SCI/ATBD/01, Issue 3, Rev. 0, 17 May 2010, 2010.

Pal, J. S., Giorgi, F., Bi, X., Elguindi, N., Solmon, F., Gao, X., Francisco, R., Zakey A., Winter, J., Ashfaq, M., Syed, F. S., Sloan, L. C., Bell, J. L., Diffenbaugh, N. S., Karmacharya, J., Konaré, A., Martinez, D., da Rocha, R. P., and Steiner, A. L.: Regional Climate Modeling for the Developing World: The ICTP RegCM3 and RegCNET, B. Am. Meteorol. Soc., 88, 1395-1409, 2007.

Posselt, R., Mueller, R., Stöckli, R., Trentmann, J.: Remote sensing of solar surface radiation for climate monitoring-The CM-SAF retrieval in international comparison, Remote Sens. of Environ., 118, 186-198, doi:10.1016/j.rse.2011.11.016, 2012.

Posselt, R., Mueller, R., Stöckli, R., Trentmann, J.: Spatial and temporal homogeneity of solar surface irradiance across satellite generations, Remote Sensing, 3, 1029-1046, 2011a.

Posselt, R., Müller, R., Stöckli, R., and Trentmann, J.: CM SAF surface radiation MVIRI Data Set 1.0 - monthly means/daily means/hourly means. Satellite application facility on climate monitoring, available at: www.cmsaf.eu, doi:10.5676/EUM_SAF_CM/RAD_MVIRI/V001, 2011b.

Posselt, R., Müller, R., Trentmann, J., Stöckli, R., Liniger, M.A.: A surface radiation climatology across two Meteosat satellite generations, Remote Sens. of Environ., 142, 103-110, doi:10.1016/j.rse.2013.11.007, 2014.

Ramanathan, V., Crutzen, P. J., Kiehl, J. L., and Rosenfeld, D.: Aerosols, climate, and the hydrological cycle, Science, 294, 2119–2124, doi:10.1126/science.1064034, 2001.

1 Ricchiazzi, P., Yang, S., Gautier, C., and Sowle, D.: SBDART: A research and Teaching
2 software tool for plane-parallel radiative transfer in the Earth's atmosphere, B. Am. Meteor.
3 Soc., 79, 2101-2114, 1998.

4 Roebeling, R., Feijt, A., and Stammes, P.: Cloud property retrievals for climate monitoring:
5 implications of differences between Spinning Enhanced Visible and Infrared Imager
6 (SEVIRI) on METEOSAT-8 and Advanced Very High Resolution Radiometer (AVHRR) on
7 NOAA-17, J. Geophys. Res., 111, D20210, doi:10.1029/2005JD006990, 2006.

8 Rummukainen, M.: State-of-the-art with regional climate models, Wiley Interdiscip. Rev.
9 Clim. Chang., 1(1), 82–96, doi:10.1002/wcc.8, 2010.

10 Rutan, D., Rose, F., Roman, M., Manalo-Smith, N., Schaaf, C., and Charlock, T.:
11 Development and assessment of broadband surface albedo from Clouds and the Earth's
12 Radiant Energy System Clouds and Radiation Swath data product, J. Geophys. Res., 114,
13 D08125, doi:10.1029/2008JD010669, 2009.

14 Sánchez-Lorenzo, A., Wild, M., and Trentmann, J.: Validation and stability assessment of the
15 monthly mean CM SAF surface solar radiation dataset over Europe against a homogenized
16 surface dataset (1983-2005), Remote Sens. Environ., 134 355-366,
17 doi:10.1016/j.rse.2013.03.012, 2013.

18 Schmetz, J., Pili, P., Tjemkes, S., Just, D., Kermann, J., Rota, S., and Ratierk, A.: An
19 introduction to Meteosat Second Generation (MSG), B. Am. Meteorol. Soc., pp. 977-992,
20 2002.

21 Solmon, F., Giorgi, F., and Liousse, C.: Aerosol modelling for regional climate studies:
22 application to anthropogenic particles and evaluation over a European/African domain, Tellus
23 B, 58, 51-72, doi:10.3402/tellusb.v58i1.16792, 2006.

24 Stengel, M., Kniffka, A., Meirink, J. F., Lockhoff, M., Tan, J., and Hollmann, R.: CLAAS:
25 the CM SAF cloud property data set using SEVIRI, Atmos. Chem. Phys., 14, 4297-4311,
26 doi:10.5194/acp-14-4297-2014, 2014.

27 Stephens, G. L., Li, J., Wild, M., Clayson, C. A., Loeb, N., Kato, S., L'Ecuyer, T.,
28 Stackhouse, P. W., Lebsock, M., and Andrews, T.: An update on Earth's energy balance in
29 light of the latest global observations, Nat. Geosci., 5, 691-696, doi:10.1038/ngeo1580, 2012.

30 Tessier, R.: The Meteosat Programme, ESA Bulletin 58, 45-57, 1989.

1 Teuling, A. J., Hirschi, M., Ohmura, A., Wild, M., Reichstein, M., Ciais, P., Buchmann, N.,
2 Ammann, C., Montagnani, L., Richardson, A. D., Wohlfahrt, G., Seneviratne, S. I., Mauder,
3 M., and Foken, T.: A regional perspective on trends in continental evaporation, Geophys. Res.
4 Lett., 36, L02404, doi:10.1029/2008GL036584, 2009.

5 Trenberth, K. E., Fasullo, J. T., and Kiehl, J.: Earth's global energy budget, B. Am. Meteorol.
6 Soc., 90, 311–323, doi:10.1175/2008bams2634.1, 2009.

7 Trentmann, J., Müller, R., and Hollmann, R.: Algorithm Theoretical Basis Document, MSG
8 Surface Radiation, Satellite Application Facility on Climate Monitoring, available at:
9 www.cmsaf.eu, doi:10.5676/EUMETSAT_SAF_CM/CLAAS/V001, 2013.

10 Vautard, R., Gobiet, A., Jacob, D., Belda, M., Colette, A., Deque, M., Fernandez, J., Garcia-
11 Diez, M., Goergen, K., Guttler, I., Halenka, T., Karacostas, T., Katragkou, E., Keuler, K.,
12 Kotlarski, S., Mayer, S., van Meijgaard, E., Nikulin, G., Patarcic, M., Scinocca, J.,
13 Sobolowski, S., Suklitsch, M., Teichmann, C., Warrach-Sagi, K., Wulfmeyer, V., and Yiou,
14 P.: The simulation of European heat waves from an ensemble of regional climate models
15 within the EURO-CORDEX project, Clim. Dynam., 41, 2555-2575, doi:10.1007/s00382-013-
16 1714-z, 2013

17 Wang, K., Dickinson, R. E., Wild, M., and Liang, S.: Evidence for decadal variation in global
18 terrestrial evapotranspiration between 1982 and 2002: 2. Results, J. Geophys. Res., 115,
19 D20113, doi:10.1029/2010JD013847, 2010.

20 Wild, M. and Liepert, B.: The Earth radiation balance as driver of the global hydrological
21 cycle, Environ. Res. Lett., 5, 025203, doi:10.1088/1748-9326/5/2/025203, 2010.

22 Wild, M., Folini, D., Schär, C., Loeb, N., Dutton, E. G., and Koning-Langlo, G.: The global
23 energy balance from a surface perspective, Clim. Dyn., 40, 3107-3134, doi:10.1007/s00382-
24 012-1569-8, 2013.

25 Zakey, A. S., Giorgi, F., and Bi, X.: Modeling of sea salt in a regional climate model: fluxes
26 and radiative forcing, J. Geophys. Res., 113, D14221, doi:10.1029/2007JD009209, 2008.

27 Zakey, A. S., Solmon, F., and Giorgi, F.: Implementation and testing of a desert dust module
28 in a regional climate model, Atmos. Chem. Phys., 6, 4687-4704, doi:10.5194/acp-6-4687-
29 2006, 2006.

1 Zanis, P., Douvis, C., Kapsomenakis, I., Kioutsioukis, I., Melas, D., Pal, J. S.: A sensitivity

2 study of the Regional Climate Model (RegCM3) to the convective scheme with emphasis in

3 central eastern and southeastern Europe, Theor. Appl. Climatol., 97, 327-337, doi:

4 10.1007/s00704-008-0075-8, 2009.

5 Zanis, P., Ntogras, C., Zakey, A., Pytharoulis, I., and Karacostas, T.: Regional climate

6 feedback of anthropogenic aerosols over Europe using RegCM3, Clim. Res., 52, 267-278,

7 doi:10.3354/cr01070, 2012.

8 Zeng, X., Zhao, M., and Dickinson, R. E.: Intercomparison of bulk aerodynamic algorithms

9 for the computation of sea surface fluxes using toga coare and tao data, J. Climate, 11, 2628-

10 2644, 1998.

11 Zubler, E. M., Folini, D., Lohmann, U., Lüthi, D., Schär, C., and Wild, M.: Simulation of

12 dimming and brightening in Europe from 1958 to 2001 using a regional climate model, J.

13 Geophys. Res., 116, D18205, doi:10.1029/2010JD015396, 2011.

14

15

16

17

18

19

20

21

22

23

24

25

26

27

1 Table 1. List of the parameters being analyzed in this work, their sources, the original

2 resolution at which the data were acquired and the corresponding time periods.

Parameter	Source	Resolution	Period
SSR	CM SAF MFG	0.03º x 0.03º	2000-2005
SSR	CM SAF MSG	0.05º x 0.05º	2006-2009
CFC	CM SAF MSG	0.05º x 0.05º	2004-2009
COT	CM SAF MSG	0.05º x 0.05º	2004-2009
Re	CM SAF MSG	0.05º x 0.05º	2004-2009
AOD	MACv1	1º x 1º	Climatology
ASY	MACv1	1º x 1º	Climatology
SSA	MACv1	1º x 1º	Climatology
ALB	CERES	1º x 1º	Climatology
WV	ERA-Interim	1º x 1º	2006-2009
All above	RegCM4	50km x 50km	2000-2009

3

4

5

6

7

8

9

10

11

12

13

14

15

16

17

18

19

20

Table 2. Average RegCM4 SSR and CM SAF SSR (MSG SEVIRI) with their standard deviations (±1σ) and the corresponding Normalized Mean Bias (NMB) and Normalized Mean Error (NME) per season and region. When the difference between RegCM4 and CM SAF SSR is statistically significant at the 95% confidence level due to a two independent sample t-test, the NMB values are marked with bold letters while in the opposite case they are marked with an asterisk. Positive NMBs are marked with red color while negative NMBs with blue. ANN corresponds to annual, DJF to winter, MAM to spring, JJA to summer and SON to autumn results.

| ANN			DJF			MAM			JJA			SON		
MOD	SAT	bias (NME)	MOD	SAT	bias (NME)	MOD	SAT	bias (NME)	MOD	SAT	bias (NME)	MOD	SAT	bias (NME)
175.0±106.5	169.3±96.7	3.3 (11.1)	77.1±57.1	74.2±57.2	3.9 (11.4)	206.8±83.0	206.7±67.0	0.0* (11.4)	281.6±70.6	265.2±55.2	6.2 (11.1)	126.3±77.4	123.3±71.3	2.4 (10.5)
173.1±106.9	171.9±97.2	0.7 (11.2)	78.1±61.0	78.0±60.8	0.1* (12.0)	202.7±85.7	208.7±68.6	-2.9 (12.3)	278.6±71.7	267.0±55.0	4.4 (10.2)	124.9±79.0	126.1±72.8	-0.9 (11.1)
178.2±105.6	164.9±95.7	8.1 (11.0)	75.3±49.7	67.7±49.8	11.3 (10.6)	213.8±77.8	203.2±64.2	5.2 (10.0)	286.7±68.2	262.1±55.3	9.4 (12.7)	128.7±74.5	118.6±68.4	8.4 (9.3)
104.0±81.2	113.7±93.4	-8.5 (16.6)	19.3±12.0	12.7±16.8	52.4 (18.3)	137.6±53.4	160.4±60.8	-14.2 (19.8)	198.7±45.5	219.4±43.3	-9.4 (13.7)	52.9±38.2	53.4±44.3	-1.0* (17.7)
134.5±89.2	136.1±83.1	-1.2 (14.2)	42.3±20.8	42.8±24.4	-1.1* (16.6)	158.1±55.6	174.0±51.3	-9.1 (13.4)	245.6±47.9	228.9±38.2	7.3 (13.2)	84.4±46.8	90.9±48.2	-7.2 (16.9)
132.3±92.0	139.5±89.8	-5.2 (14.4)	37.5±17.5	38.8±22.1	-3.4 (19.1)	155.2±61.2	179.4±57.7	-13.5 (16.5)	248.4±44.9	242.8±36.5	2.3 (10.7)	80.1±46.0	88.8±48.8	-9.8 (17.6)
197.9±95.1	194.7±84.4	1.7 (11.2)	91.7±26.9	98.6±27.5	-7.0 (14.7)	224.8±56.5	224.0±46.3	0.4* (12.0)	317.5±29.1	296.3±32.3	7.2 (9.9)	148.6±53.9	151.8±50.4	-2.1 (10.3)
209.8±98.6	195.1±85.1	7.5 (9.9)	97.3±29.1	96.7±27.1	0.6* (10.6)	243.7±59.2	225.9±46.2	7.9 (8.7)	331.3±27.3	299.9±25.1	10.4 (10.5)	157.7±53.5	149.8±45.4	5.3 (9.8)
219.3±101.6	205.6±90.3	6.7 (9.0)	105.1±36.8	101.8±33.7	3.3 (11.3)	251.4±68.8	235.6±54.4	6.7 (9.7)	339.3±29.1	312.8±28.1	8.5 (8.0)	171.8±63.0	163.7±55.9	5.0 (8.4)
261.8±82.3	243.8±69.5	7.4 (6.9)	164.7±35.2	161.8±31.9	1.8 (7.1)	303.8±41.3	280.2±33.7	8.4 (5.9)	353.5±20.5	320.5±21.6	10.3 (8.1)	217.2±49.5	205.8±39.7	5.5 (6.4)

1   Table 3. Normalized Mean Bias (NMB) of RegCM4-CM SAF Rel and Rei, RegCM4-MACv1

2   ASY and SSA, RegCM4-CERES ALB and RegCM4-ERA-Interim WV. When the difference

3   between RegCM4 and CM SAF or CERES or ERA-Interim is statistically significant at the

4   95% confidence level due to a two independent sample t-test, the NMB values are marked

5   with bold letters while in the opposite case they are marked with an asterisk. Positive NMBs

6   are marked with red color while negative NMBs with blue.

	CFC	COT	Rel	Rei	AOD	ASY	SSA	ALB	WV
EU	-24.3	4.3	-36.1	-28.3	-35.3	-1.1	-4.2	1.6	12.0
LA	-13.7	7.3	-47.7	-26.4	-32.1	-1.8	-4.3	-28.3	11.4
OC	-38.4	-2.5	-18.3	-31.1	-42.0	0.1	-4.1	131.1	12.8
NE	-20.3	54.3	-32.8	-31.3	-75.9	1.0	-5.6	5.2	13.1
CE	-19.7	24.1	-45.1	-24.0	-63.6	0.0*	-5.9	-22.7	14.0
EE	-16.0	30.8	-44.6	-24.2	-64.6	2.1	-3.5	-40.7	10.8
IP	-13.7	-13.9	-46.1	-27.3	-7.4	-1.5	-4.8	-3.8	14.4
CM	-31.2	-30.7	-26.7	-27.6	-19.3	-0.7	-3.5	85.9	10.4
EM	-28.8	-22.0	-29.3	-28.4	-34.2	-0.0	-2.3	35.4	10.9
NA	0.4*	-39.8	-47.3	-30.0	25.0	-7.9	-3.5	-26.4	8.7

7

8

9
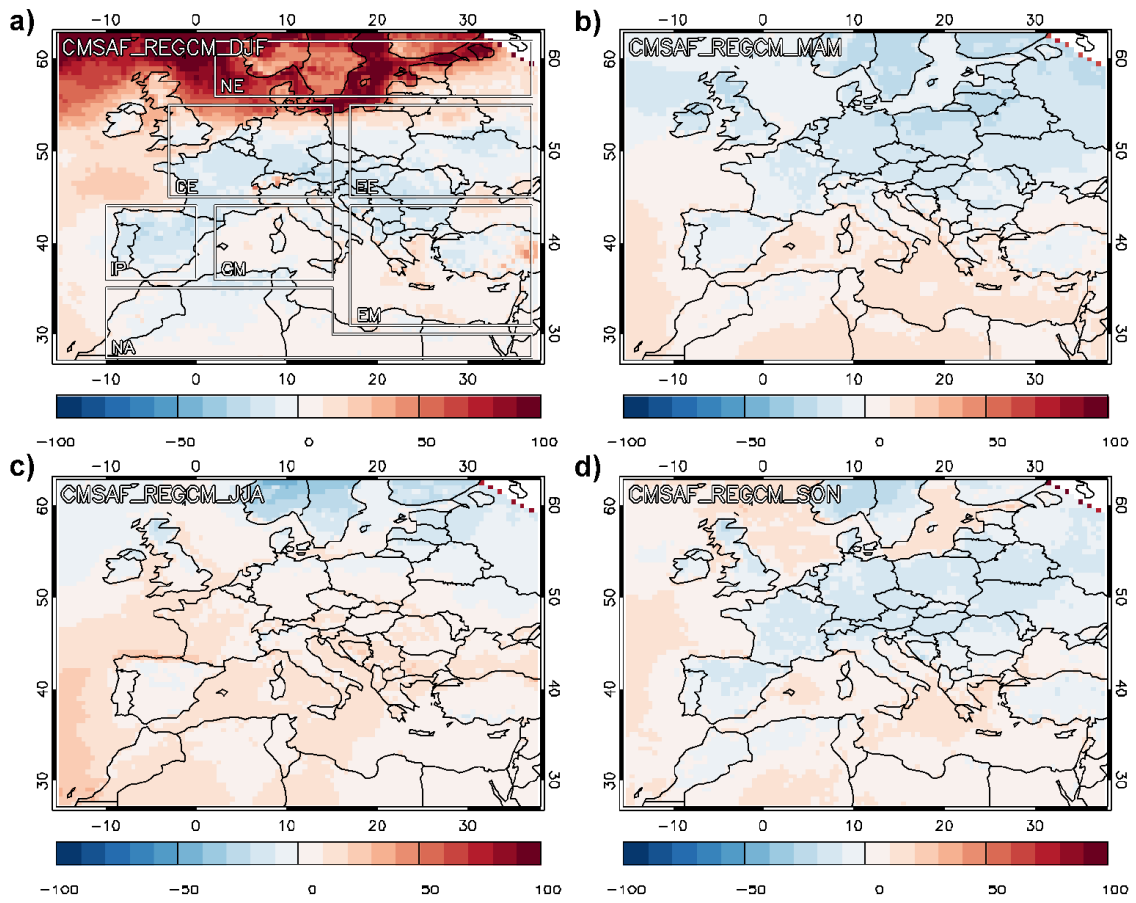
Figure 1. Seasonal NMB patterns of RegCM4-CM SAF SSR over Europe for (a) winter (DJF), (b) spring (MAM), (c) summer (JJA) and (d) autumn (SON) from MSG SEVIRI observations. The 7 sub-regions used for the generalization of the results are marked in Fig. 1a: Northern Europe (NE), Central Europe (CE), Eastern Europe (EE), Iberian Peninsula (IP), Central Mediterranean (CM), Eastern Mediterranean (EM) and Northern Africa (NA).
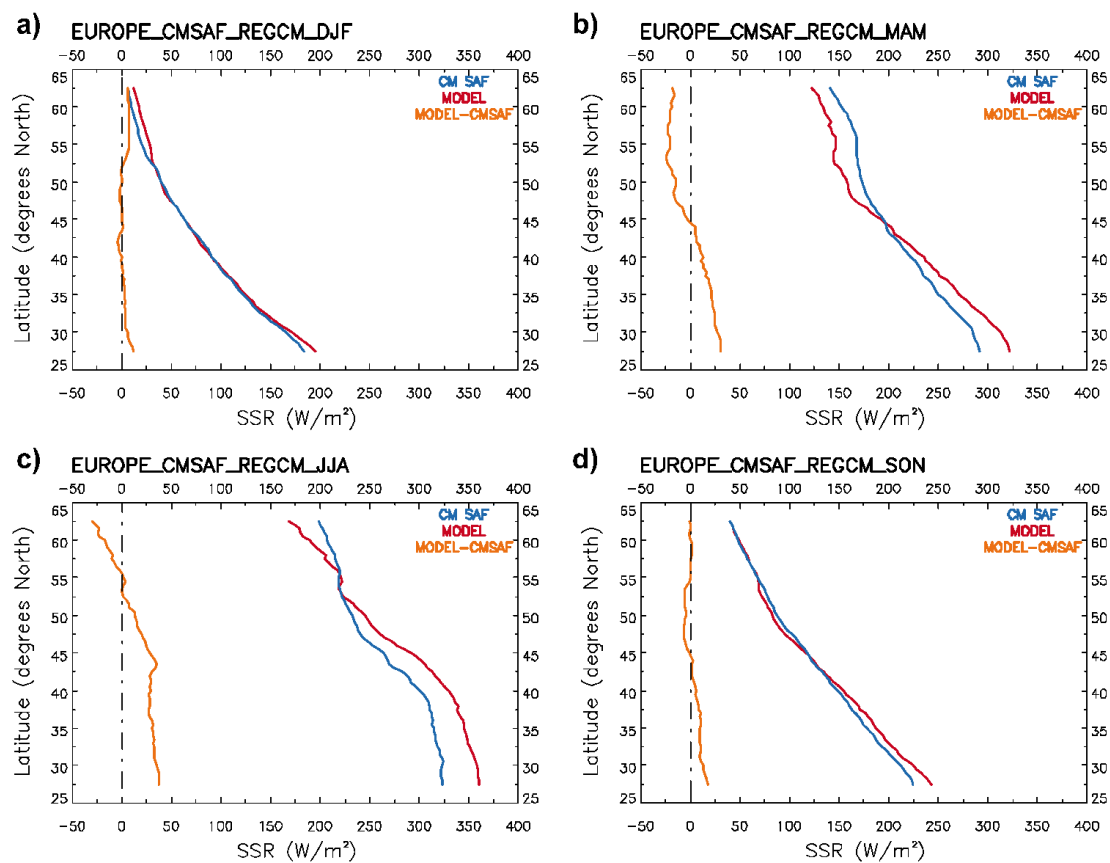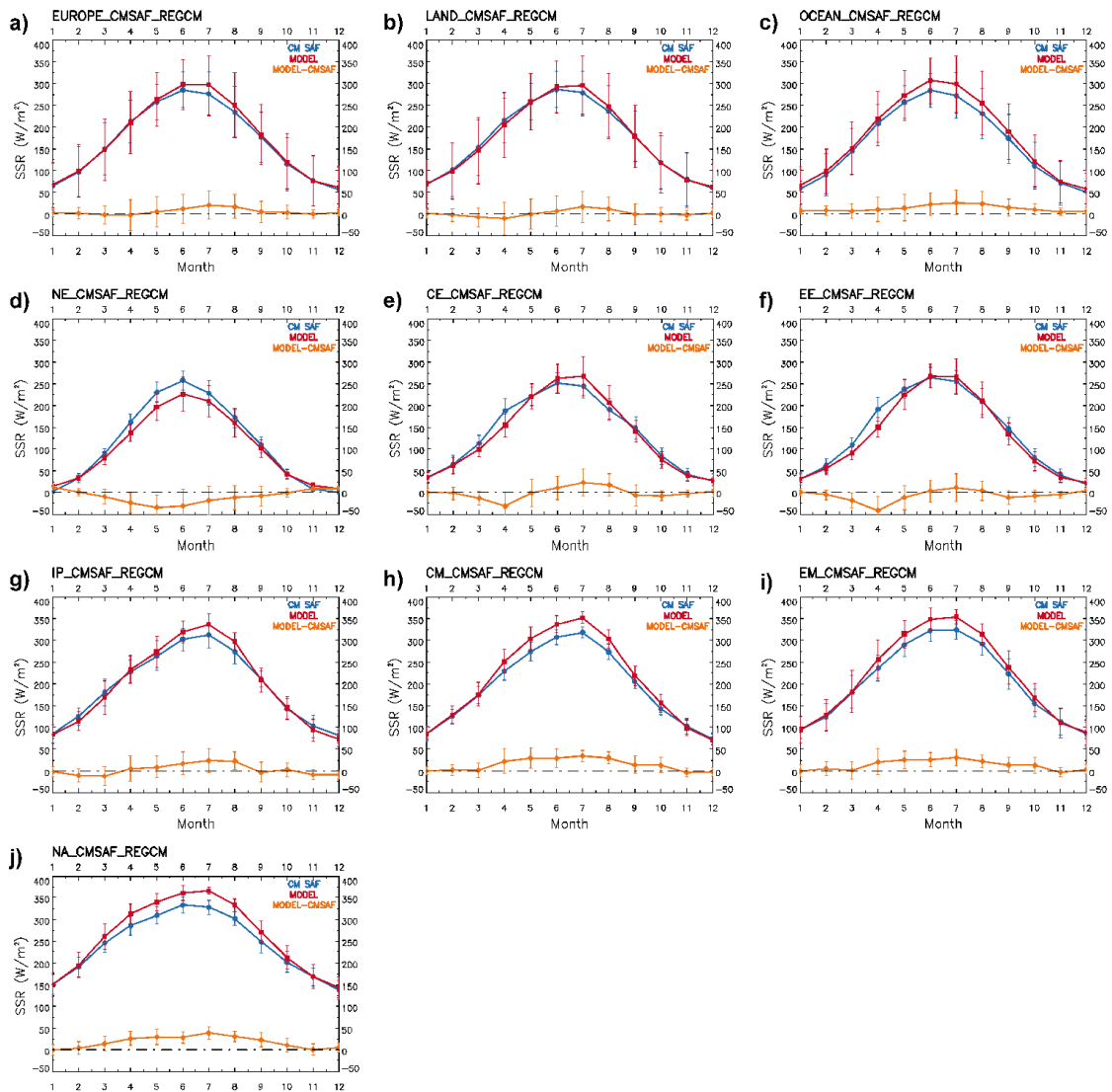
Figure 2. Latitudinal variability of RegCM4 SSR (red), CM SAF SSR (blue) and their difference (orange) over Europe for (a) winter (DJF), (b) spring (MAM), (c) summer (JJA) and (d) autumn (SON) from MSG SEVIRI observations.

1

2

Figure 3. Seasonal variability of RegCM4 SSR (red), CM SAF SSR (blue) and their difference (orange) over (a) the whole Europe, (b) Land, (c) Ocean, (d) NE, (e) CE, (f) EE, (g) IP, (h) CM, (i) EM, (j) NA from MSG SEVIRI observations.

6

7

8

9
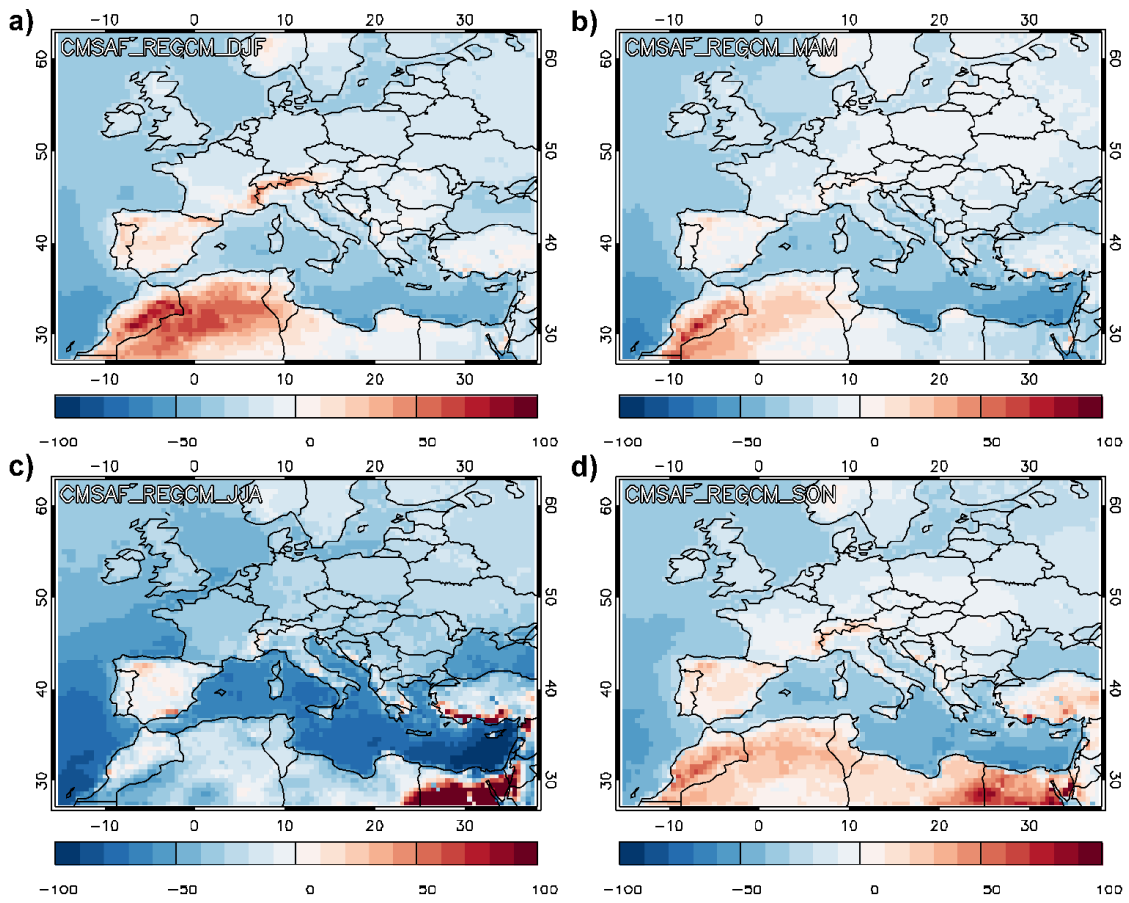
Figure 4. The same as Fig. 3 but for RegCM4 and CM SAF CFC.

1

2
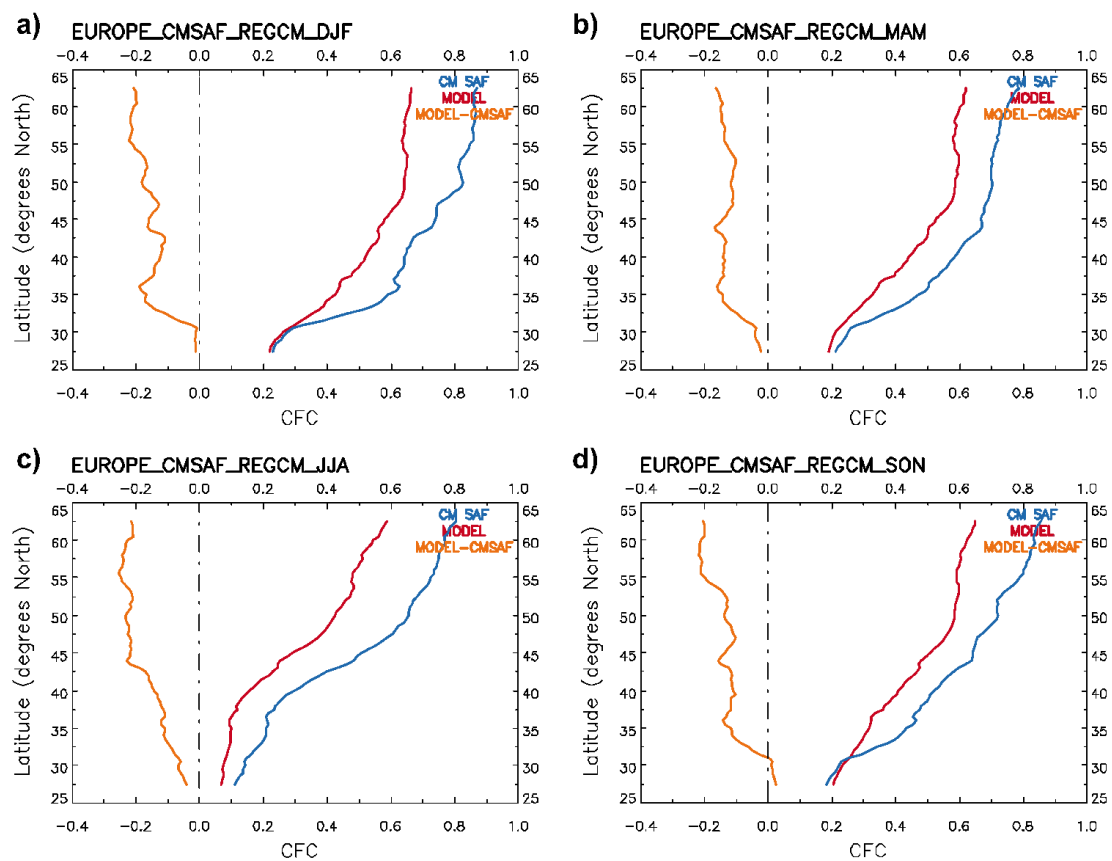
3   Figure 5. The same as Fig. 4 but for RegCM4 and CM SAF CFC.

4

5

6

7

8

9

10

11

12

13

14
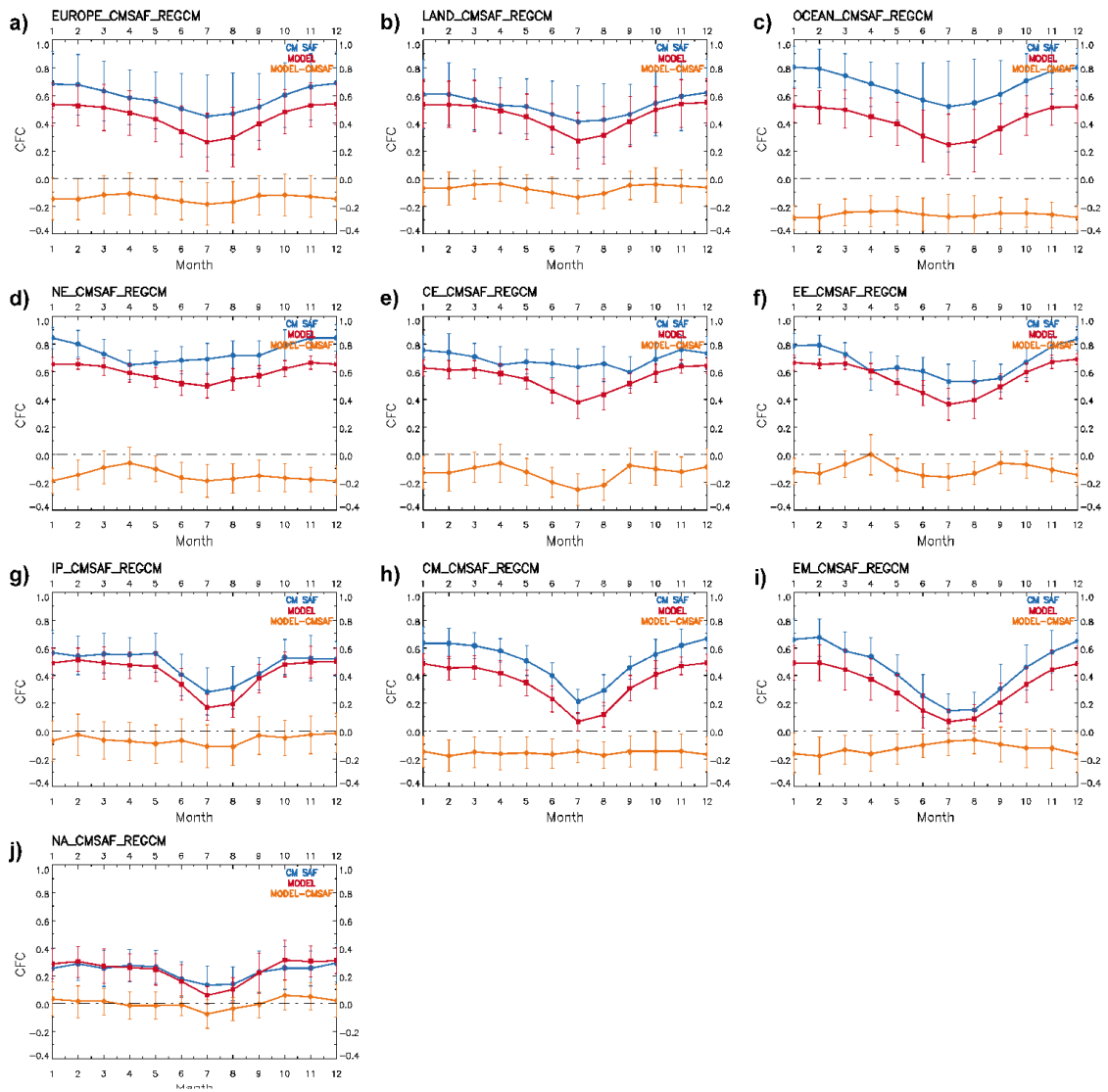
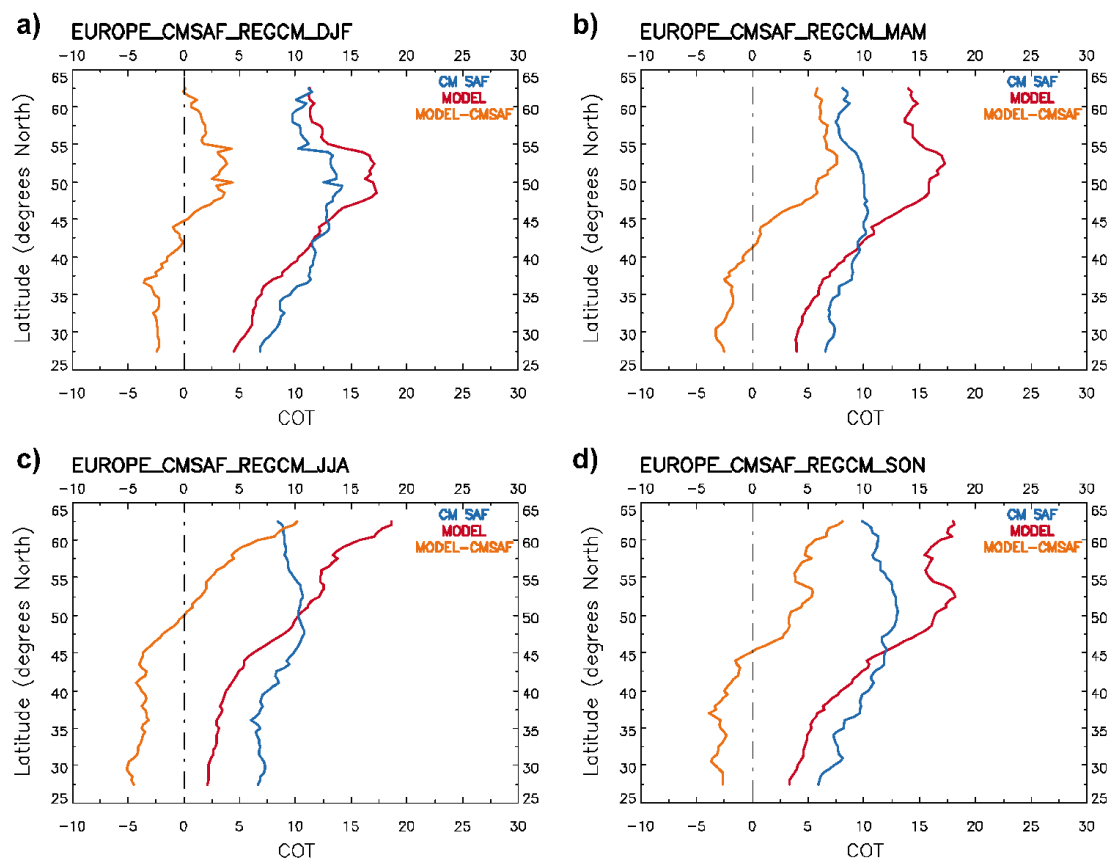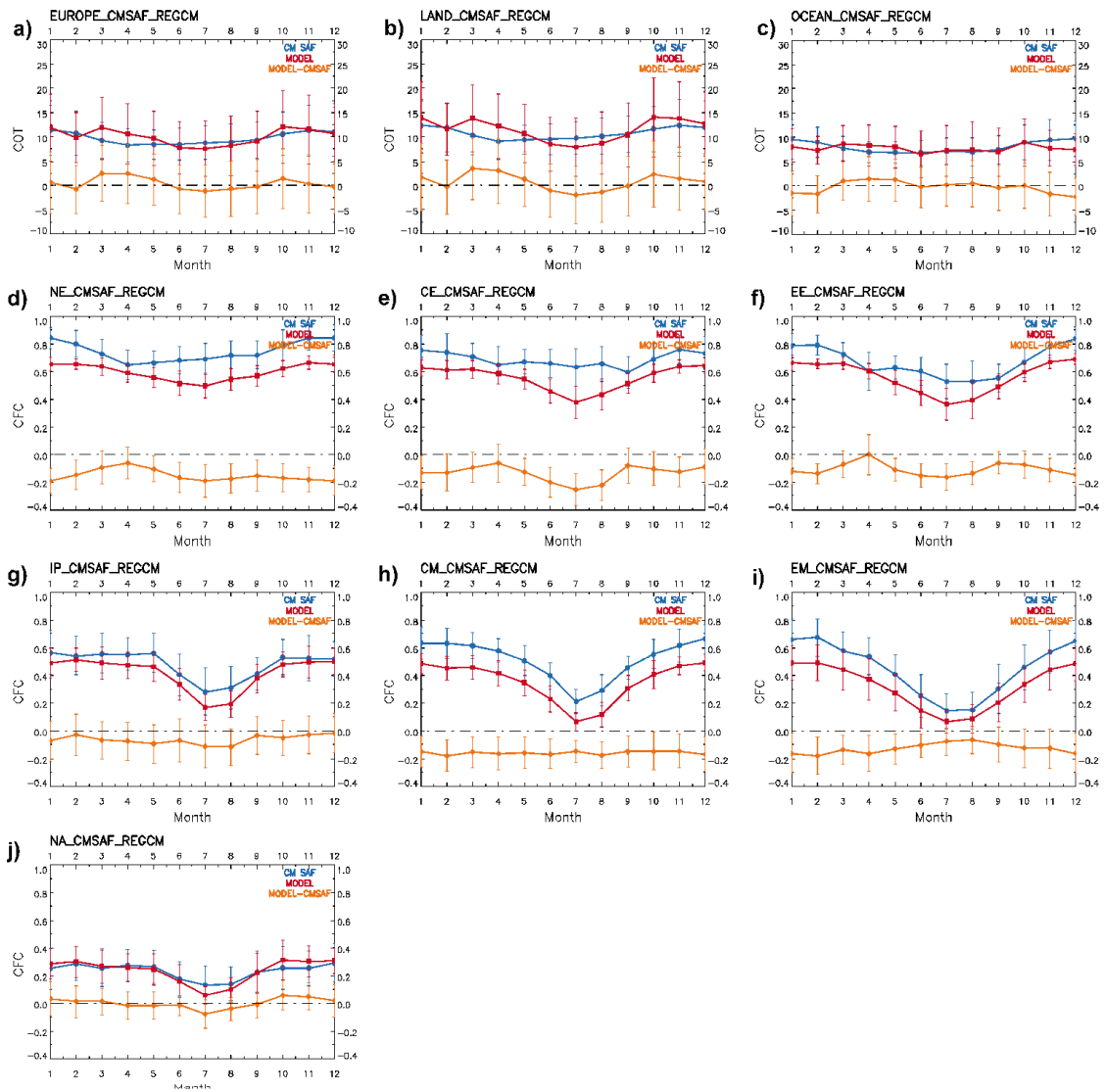Figure 6. The same as Fig. 5 but for RegCM4 and CM SAF CFC.
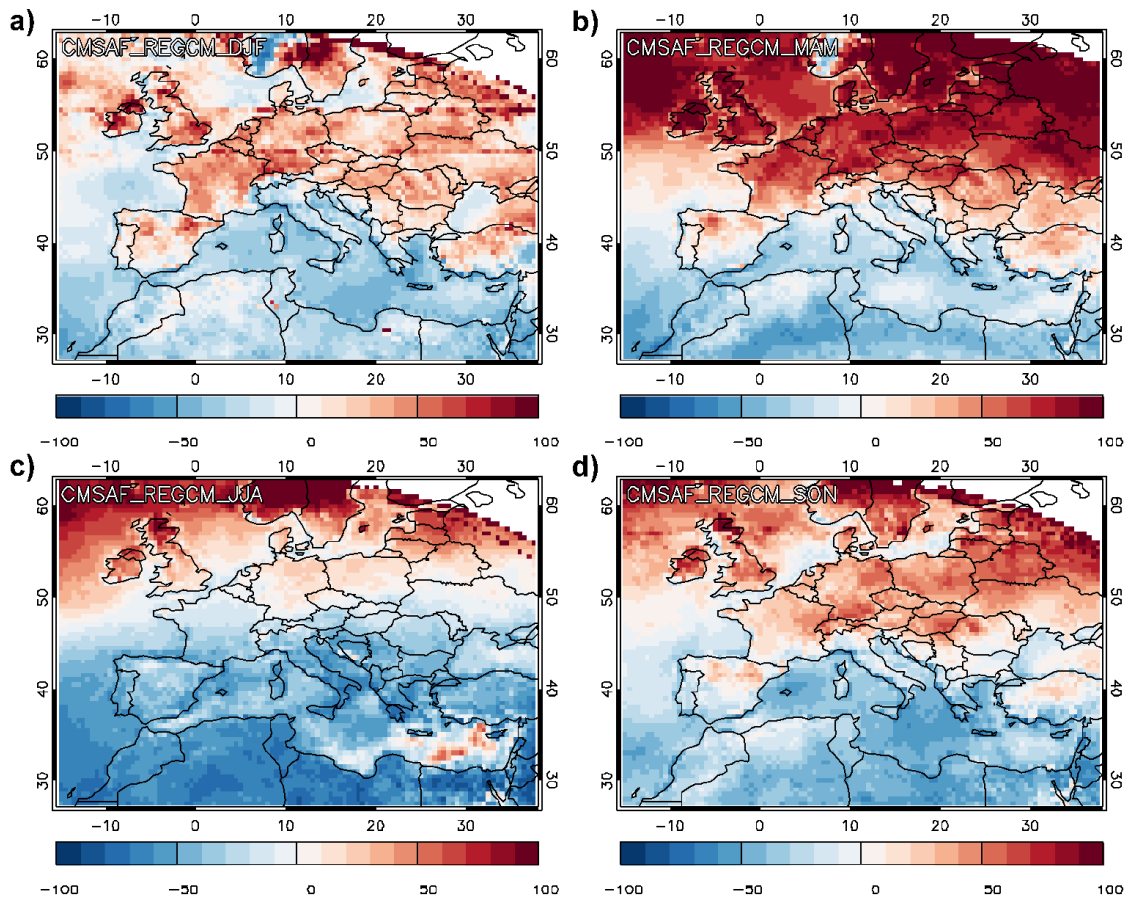
Figure 7. The same as Fig. 3 but for RegCM4 and CM SAF COT.
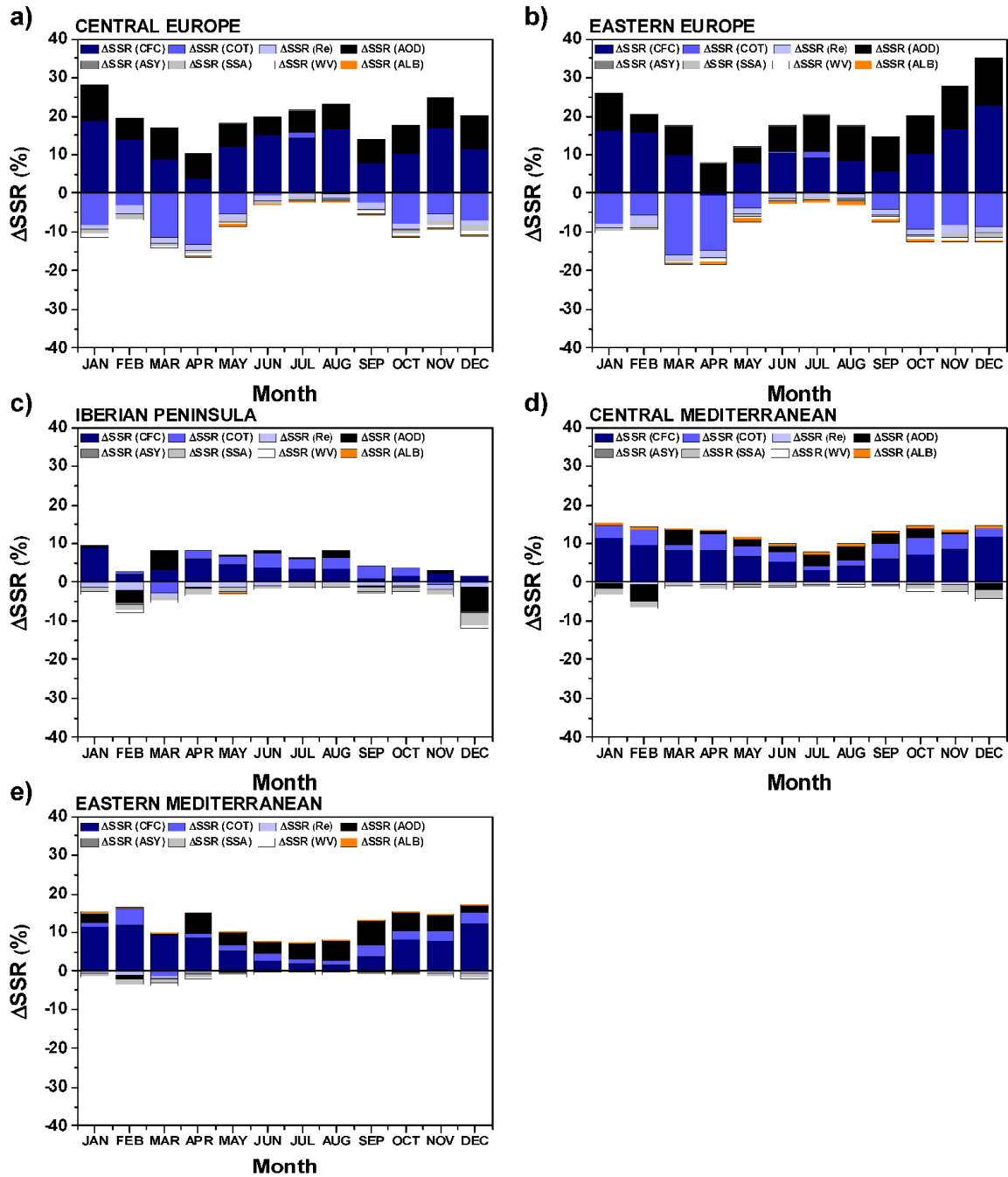
1

2

3

4

5

6

7

8

9

10

11

12

13

14

Figure 8. The same as Fig. 4 but for RegCM4 and CM SAF COT.

1

2

3   Figure 9. The same as Fig. 5 but for RegCM4 and CM SAF COT.

4

5

6

7

8

9

10

11

Figure 10. ΔSSR (%) caused by CFC, COT, Re, AOD, ASY, SSA, WV and ALB for (a) CE, (b) EE, (c) IP, (d) CM and (e) EM.